REPORT 996

FREE-SPACE OSCILLATING PRESSURES NEAR THE TIPS OF ROTATING PROPELLERS

By HARVEY H. HUBBARD and ARTHUR A. REGIER

SUMMARY

The theory is given for calculating the free-space oscillating pressures associated with a rotating propeller, at any point in space. Because of its complexity this analysis is convenient only for use in the critical region near the propeller tips where the assumptions used by Gutin to simplify his final equations are not valid. Good agreement was found between analytical and experimental results in the tip Mach number range 0.45 to 1.00 where static tests were conducted. Charts based on experimental data are included for the fundamental frequencies of two-, three-, four-, five-, six-, and eight-blade propellers and for a range of tip clearances from 0.04 to 0.30 times the propeller diameter. If the power coefficient, tip Mach number, and the tip clearance are known for a given propeller, the designer may determine from these charts the average maximum free-space oscillating pressure in the critical region near the plane of rotation. A section of the present report is devoted to the fuselage response to these oscillating pressures and indicates some of the factors to be considered in solving the problems of fuselage vibration and noise.

Pressures in the region ahead of the plane of rotation tended to be out of phase with those behind it. A reflector in the pressure field increased pressures in the plane of its surface by an amount which depended on its shape; a flat surface caused a doubling of the free-space values. Blade plan form is shown not to be a significant parameter. The nondimensional parameter, tip clearance divided by propeller diameter, however, is shown to be significant. As the tip clearance was decreased, pressures in a region about as wide as one propeller radius were greatly increased. At a constant power the pressure amplitudes of the lower harmonics tended to decrease and the higher harmonics tended to increase with an increase in tip Mach number. The fundamental frequency of pressure produced by a four-blade propeller was essentially independent of tip Mach number in the useful tip Mach number range. At tip Mach numbers near 1.00, the pressure amplitudes were not appreciably reduced by increasing the number of blades; however, the resulting higher frequencies of the impinging pressures were beneficial in greatly reducing the vibration amplitude of the wall.

INTRODUCTION

Large-amplitude fuselage-wall vibrations in the region near the propeller plane have been experienced recently in several experimental airplanes. Fuselage-panel failures have occurred and great discomfort to the crew has resulted from the noise and vibration inside the airplane. These vibrations are known to result from the oscillating pressures associated with the rotating propeller. Up to the present time, however, very little information has been published that would enable a designer to predict these pressures in the critical region near the propeller tips.

In reference 1 Gutin has developed a theory by means of which the sound of a propeller may be predicted. By making several simplifying assumptions Gutin simplified the final equations, which were then useful only at a large distance from the propeller. The analysis presented herein is based on Gutin's fundamental equations without some of the simplifying assumptions of the original paper. The solution obtained then makes possible the prediction of oscillating pressures at any point in space. Its practical usefulness, however, is limited to the area close to the propeller tips, where Gutin's simplified solution is not valid. At a larger distance away the Gutin solution is much more convenient to use.

Static tests were made in which several different propeller models were used for comparison with analytical results. These tests evaluated the effects on the free-space oscillating-pressure distributions of such parameters as propeller diameter, blade plan form, number of blades, blade loading, tip clearance, and tip Mach number. Charts based on experimental data were calculated to enable a designer to estimate the average maximum free-space oscillating pressures in the critical region near the plane of rotation. Comparative data were obtained at the surface of two different simulated fuselage wall shapes to determine their effects on the free-space pressures. The fuselage response to these pressures is treated herein and indicates some of the factors to be considered in solving fuselage vibration and noise problems.

SYMBOLS

R_e	effective propeller radius
S	distance between doublet and observer
S_e	distance from observer to doublets at effective propeller radius
x, y, z	Cartesian system of coordinates, propeller axis along x-axis
x', y', z'	axes with origin at doublet and parallel to x-, y-, and z-axes
d	tip clearance
D	propeller diameter
r	station radius

b blade width
h maximum thickness of blade section
B number of blades
ρ density of air
c speed of sound
$k=\frac{mB\omega}{c}$
M_t tip Mach number (rotation only)
R tip radius of propeller
Q torque
T thrust
P power
p_i instantaneous pressure for a given harmonic $\left(\rho\frac{\partial\phi}{\partial t}\right)$
p free-space oscillating pressure for a given harmonic, root-mean-square
$\overline{p}$ total free-space oscillating pressure, root-mean-square $\left(\sqrt{\sum_{m=1}^{m=\infty} p_{mB}^2}\right)$
p_{mB} p for any mB value
p_s pressure at panel surface
ω rotational speed, radians per second
ω_n undamped natural angular frequency of vibration of panel, radians per second
ω_1 angular frequency of sound or vibration, radians per second
t time, seconds
n propeller rotational speed, revolutions per second
C_T thrust coefficient $\left(\frac{T}{\rho n^2 D^4}\right)$
$W=(C+2K)+i\left(M\omega_1-\frac{s}{\omega_1}\right)$
C_Q torque coefficient $\left(\frac{Q}{\rho n^2 D^5}\right)$
C_P power coefficient $\left(\frac{P}{\rho n^3 D^5}\right)$
$\overline{p}_c$ total free-space oscillating pressure coefficient $\left(\frac{\overline{p}}{\rho n^2 D^2}\right)$
p_c free-space oscillating pressure coefficient $\left(\frac{p}{\rho n^2 D^2}\right)$
m order of the harmonic
$A(r)=\frac{1}{B}\frac{dT}{dr}$
$F(r)=\frac{1}{Br}\frac{dQ}{dr}$
ϵ_m phase angle between Fourier harmonic of impulse and torque component of impulse
η_m phase angle between Fourier harmonic of impulse and thrust component of impulse
β blade angle, degrees
δ angle of doublet from observer with respect to x' axis
χ angle of doublet from observer with respect to y' axis
ν angle of doublet from observer with respect to z' axis
ϕ velocity potential
θ angle between y-axis and radius of doublet circle
ξ_{01} amplitude of impinging free wave
$\dot{\xi}_{01}$ velocity of impinging free wave
ξ_{02} amplitude of panel vibration
$\dot{\xi}_{02}$ velocity of panel vibration
C structural damping of wall
C_c critical structural damping $(2M\omega_n)$
K acoustical radiation resistance (ρc)
M mass of panel per unit area
s effective stiffness of panel per unit area $(M\omega_n^2)$
T_c transmission coefficient $(\xi_{02}/\xi_{01})^2$
A_c absorption coefficient
f_1 frequency of sound or vibration, cycles per second
f_0 natural frequency of panel, cycles per second

A dot over a quantity indicates the first derivative with respect to time of that quantity.

THEORY

The theory for the generation of sound by a propeller is given by Gutin in reference 1. His basic assumptions are that the propeller is replaced by concentrated forces or acoustic doublets distributed over the propeller disk, the strength of the doublets being a function of the torque and thrust of the propeller. By considering only the sound at a great distance from the propeller, Gutin could make further simplifying assumptions which permitted a solution in terms of Bessel functions. In the present analysis, which considers the oscillating pressures near the propeller tips, the assumptions of great distance cannot be made. The analysis therefore follows closely that of Gutin, with the exception that no simplifying assumption as to distance is made.

Certain geometric relations used in the analysis are shown in figure 1. The propeller lies in the zy-plane and the observer is in the xy-plane. The radius of a doublet circle is r. The doublet under consideration is located at the origin of the primed coordinates with angles to observer indicated by δ, χ, and ν. The distance between the observer and the doublet is S. The coordinates of the observer in the primed coordinate system are

$$x'=x$$

$$y'=y-r\cos\theta$$

$$z'=-r\sin\theta$$

Therefore,

$$S=\sqrt{x^2+y^2+r^2-2ry\cos\theta}$$

and

$$\cos\delta=\frac{x}{S}$$

$$\cos\chi=\frac{y-r\cos\theta}{S}$$

$$\cos\nu=\frac{-r\sin\theta}{S}$$

Reference 1 shows that the velocity potential for a given harmonic due to concentrated forces distributed over the propeller disk is given by the following expression:

$$\phi=\frac{iB}{4\pi^2\rho ck}\int_0^R\int_0^{2\pi}[A(r)e^{i(kct-mB\theta-\epsilon_m)}\cos\delta+$$

$$F(r)e^{i(kct-mB\theta-\eta_m)}(\cos\chi\sin\theta-\cos\nu\cos\theta)]\frac{\partial}{\partial S}\left(\frac{e^{-ikS}}{S}\right)dr\,d\theta$$

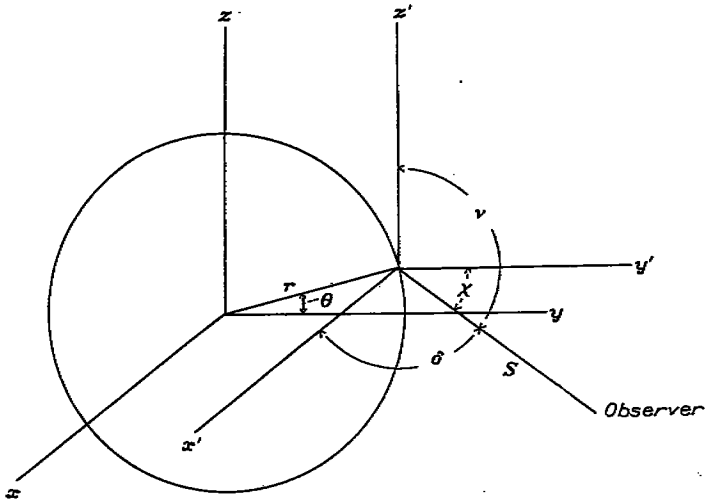

FIGURE 1.—Description of coordinate system.

Making the substitution for the direction cosines, evaluating $\frac{\partial}{\partial S}\left(\frac{e^{-ikS}}{S}\right)$, and dropping the small phase angles ϵ_m and η_m gives

$$\phi=\frac{-iB}{4\pi^2\rho ck}\int_0^R\int_0^{2\pi}\left[\frac{x}{S}A(r)e^{i(kct-mB\theta-kS)}+\frac{y\sin\theta}{S}F(r)e^{i(kct-mB\theta-kS)}\right]\left(\frac{ik}{S}+\frac{1}{S^2}\right)dr\,d\theta$$

When the concept of an effective radius at which the thrust and torque are assumed to act as in reference 1 is used, and when the following substitutions are also made as in reference 1

$$A(r)dr=\frac{dT}{B}$$

and

$$F(r)dr=\frac{dQ}{Br}$$

then

$$\phi=\frac{-ie^{ikct}}{4\pi^2\rho ck}\int_0^{2\pi}\left(Tx+\frac{Qy\sin\theta}{R_e}\right)\left(\frac{ikS_e+1}{S_e^3}\right)[\cos(mB\theta+kS_e)-i\sin(mB\theta+kS_e)]\,d\theta$$

where R_e is an effective radius of the propeller.

The instantaneous pressure for a given harmonic at any point is given by $p_i=\rho\frac{\partial\phi}{\partial t}$. Hence,

$$p_i=\frac{e^{ikct}}{4\pi^2}\int_0^{2\pi}\left(Tx+\frac{Qy\sin\theta}{R_e}\right)\left(\frac{ikS_e+1}{S_e^3}\right)[\cos(mB\theta+kS_e)-i\sin(mB\theta+kS_e)]\,d\theta \tag{1}$$

The absolute value of root-mean-square pressure p is given by the following expression:

$$p=\frac{1}{4\sqrt{2}\pi^2}\left(\left\{\int_0^{2\pi}\left(Tx+\frac{Qy\sin\theta}{R_e}\right)\frac{1}{S_e^3}[\cos(mB\theta+kS_e)+kS_e\sin(mB\theta+kS_e)]d\theta\right\}^2+\left\{\int_0^{2\pi}\left(Tx+\frac{Qy\sin\theta}{R_e}\right)\frac{1}{S_e^3}[kS_e\cos(mB\theta+kS_e)-\sin(mB\theta+kS_e)]d\theta\right\}^2\right)^{1/2}$$

where

$$S_e=\sqrt{x^2+y^2+R_e^2-2R_ey\cos\theta}$$

which is the distance from the observer to the doublets of the effective propeller circle.

This expression for p may be written in nondimensional form as

$$\frac{p}{\rho n^2D^2}=\frac{1}{4\sqrt{2}\pi^2}\left(\left\{\int_0^{2\pi}\left(\frac{C_TD^2x}{S_e^3}+\frac{C_QD^3y\sin\theta}{R_eS_e^3}\right)[\cos(mB\theta+kS_e)+kS_e\sin(mB\theta+kS_e)]\,d\theta\right\}^2+\left\{\int_0^{2\pi}\left(\frac{C_TD^2x}{S_e^3}+\frac{C_QD^3y\sin\theta}{R_eS_e^3}\right)[kS_e\cos(mB\theta+kS_e)-\sin(mB\theta+kS_e)]\,d\theta\right\}^2\right)^{1/2} \tag{2}$$

where p is the magnitude of the root-mean-square oscillating pressure of a given harmonic. The quantity $\frac{p}{\rho n^2 D^2}$ is defined as the free-space oscillating-pressure coefficient and is designated p_c. The total free-space oscillating pressure is given by the expression $\overline{p}=\sqrt{\sum_{m=1}^{m=\infty} p_{mB}{}^2}$ where p for any mB value is given by equation (2) and the total free-space oscillating-pressure coefficient is defined as $\overline{p}_c=\frac{\overline{p}}{\rho n^2 D^2}$.

APPARATUS AND METHODS

Static tests were conducted for the measurement and analysis of the free-space pressures near the tips of five different propeller models. Tests were made in the tip Mach number range 0.45 to 1.00 for 2 two-blade 48-inch-diameter round-tip propellers, a four-blade 48-inch-diameter round-tip propeller, a two-blade 47-inch-diameter square-tip propeller, and a two-blade 85-inch-diameter round-tip propeller and for various blade angles. Comparative studies were also made to determine the effects on free-space pressures of a flat vertical wall and a curved surface which simulate the fuselage position in the pressure field.

Propeller models used are shown in figure 2. These models were mounted in adjustable hubs to allow the blade angles to be changed manually. The 85-inch-diameter Clark Y propeller, the NACA 4–(3)(06.3)–06 propeller, the NACA 4–(5)(08)–03 propeller, and the square-tip propeller were all tested as two-blade configurations. The NACA 4–(5)(08)–03 propeller was also tested as a four-blade configuration. The square-tip propeller blade shown has the same airfoil section as the NACA 4–(5)(08)–03 propeller and its diameter is 47 inches. The NACA designations are descriptive of the propeller. Numbers in the first group represent the propeller diameter in feet. Numbers in the first parentheses represent the design lift coefficient in tenths at the 0.7 radius. Numbers in the second parentheses give the blade thickness at the 0.7 radius in percent chord. The last group of numbers gives the blade solidity which is defined as the ratio of a single blade width at the 0.7 radius to the circumference of a circle with the same radius. Blade-form curves for the four models tested are given in figure 3.

The test propellers were driven by a 200 horsepower water-cooled variable-speed electric motor. Power to the motor was measured by means of a wattmeter, and motor-efficiency charts were used to determine power to the propellers.

Root-mean-square oscillating pressures were measured by means of a commercial crystal type microphone calibrated to read directly in dynes per square centimeter. The sensitive element has a flat frequency response in the desired range and is approximately ⅝ inch in diameter; thus, any distortion of the pressure field due to its presence is minimized. Figure 4 shows the test arrangement for measuring free-space pressures. Because ground reflection is considered negligible for this particular setup, the pressures measured are essentially free-space pressures except in the cases where reflecting surfaces were purposely placed in the pressure field. All pressure quantities presented are considered to be free-space oscillating pressures unless otherwise stated.

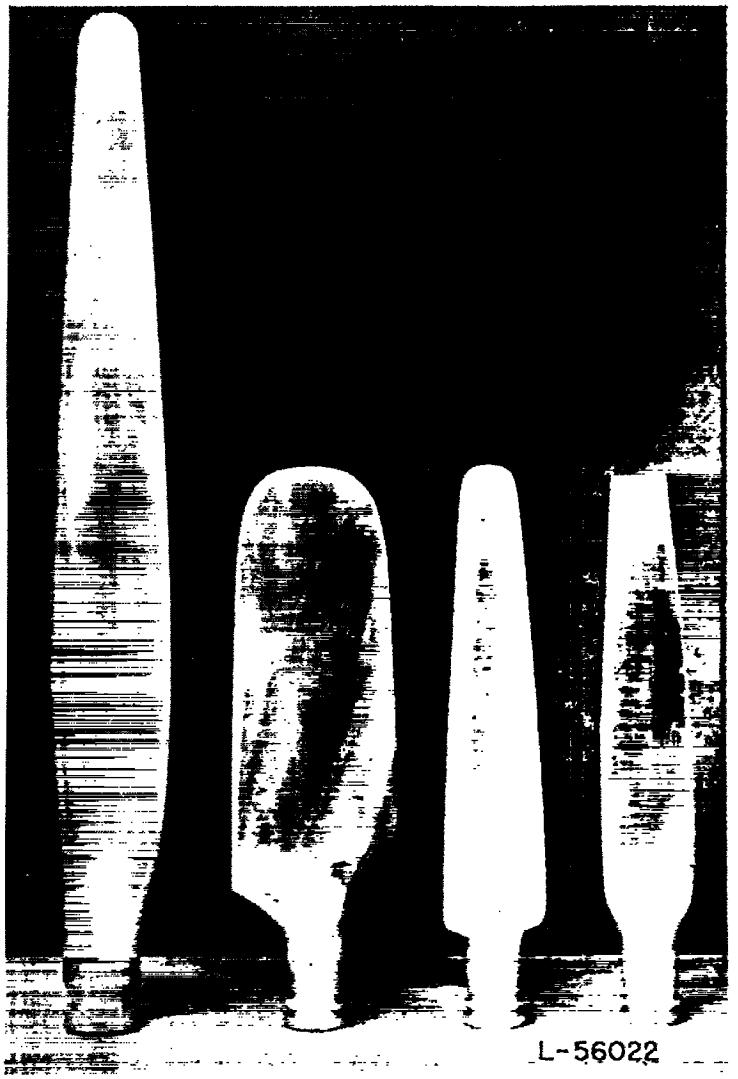

FIGURE 2.—Propeller test blades.

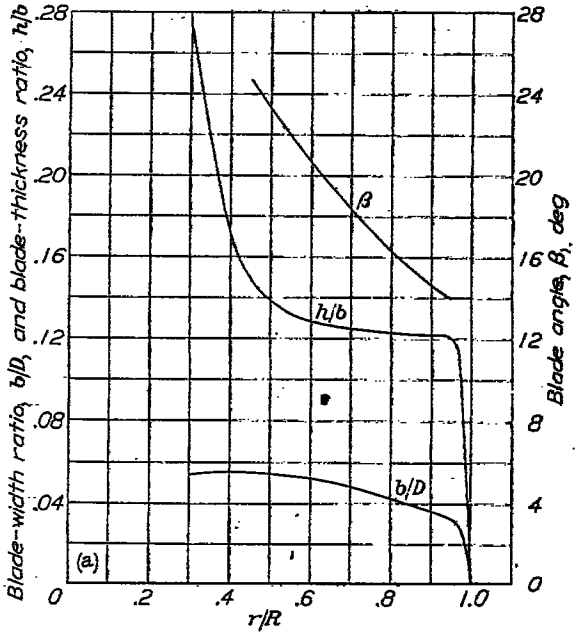

(a) Clark Y propeller.

FIGURE 3.—Blade-form curves for test propellers.

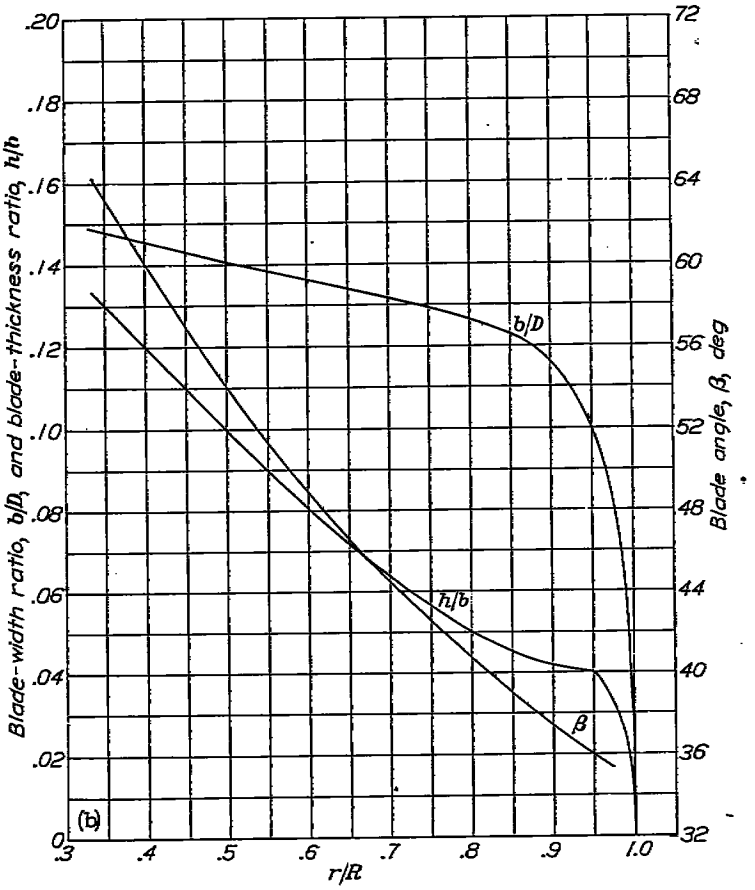

(b) NACA 4-(3)(06.3)-06 propeller.

FIGURE 3.—Continued.

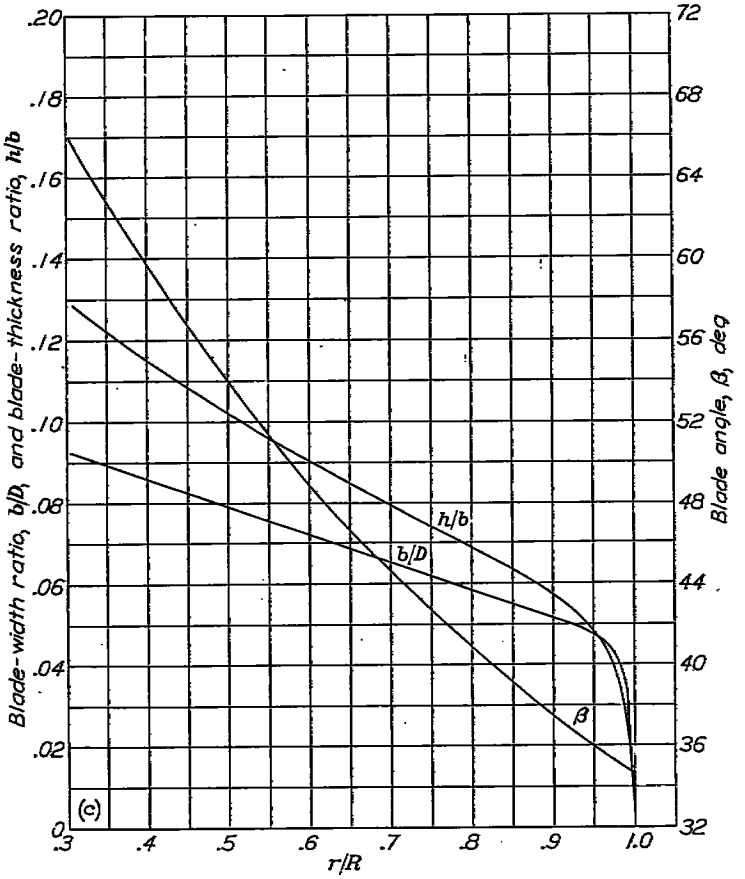

(c) NACA 4-(5)(08)-03 propeller.

FIGURE 3.—Continued.

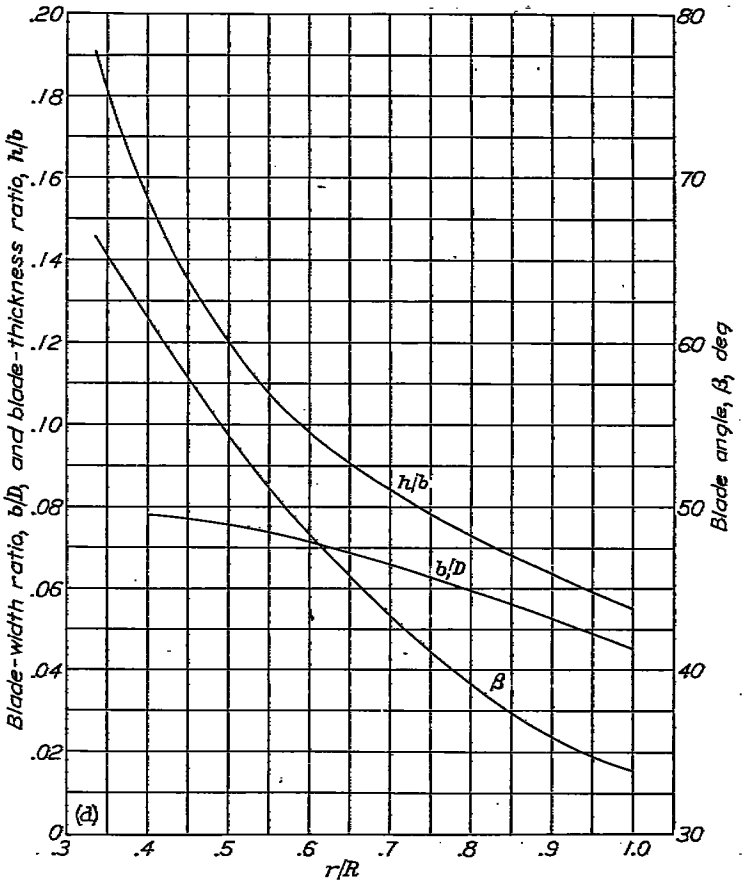

(d) Square-tip propeller.

FIGURE 3.—Concluded.

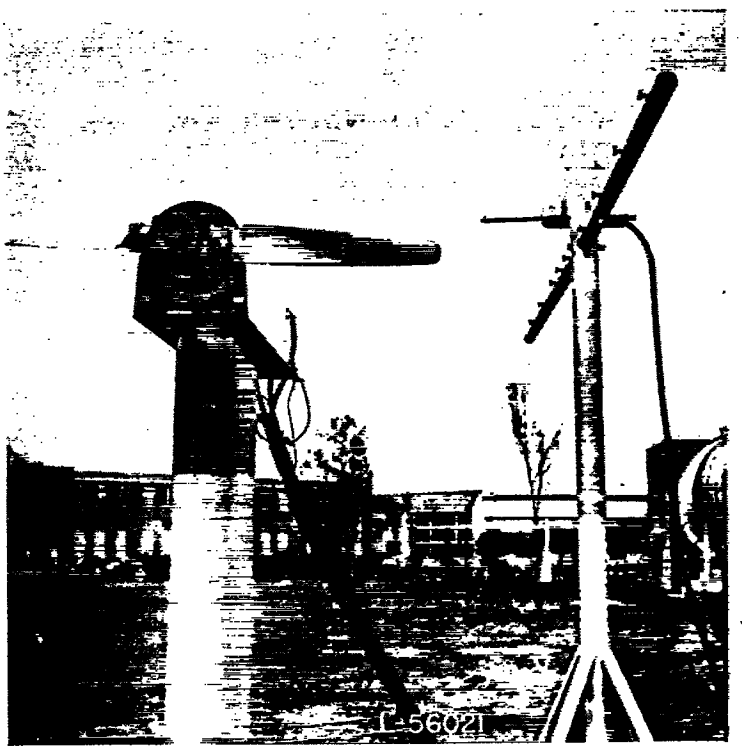

FIGURE 4.—Test setup for free-space pressure measurements.

Measurements were made at several known distances from the propeller on lines parallel to the axis of rotation and at the same height above ground. At all times the microphone was doubly shock-mounted and when reflecting surfaces were used the microphone was mounted separately to keep vibrations reaching it at a minimum.

Pressure amplitudes (rms) of the first four harmonics were measured with a harmonic wave analyzer adjusted to a band width of 100 cycles per second.

Flat vertical and circular fuselage walls were simulated and their effects on the magnitudes of pressures in the plane of the walls were evaluated. Figures 5 (a) and 5 (b) show construction of the flat vertical wall and figure 5 (c) shows corresponding details of the circular wall. These walls were supported in such a way that the natural frequency of each structure as a unit was below the frequency range of the oscillating pressures to be measured. As first designed the surfaces of both walls vibrated locally when excited by the propeller frequencies. These local (panel) vibrations were reduced in both cases to a low value by heavy longitudinal reinforcement. By this method panel resonances were removed from the frequency range where measurements were to be taken.

The vertical dimension of both walls was 3 feet which was assumed sufficient to approximate an actual fuselage for use with a 4-foot propeller. The reinforced wooden (two thicknesses of ¾-in. plywood) wall was 6 feet long and weighed approximately 145 pounds, whereas the reinforced steel (3/32-in. boiler plate) wall was 4 feet long and weighed approximately 100 pounds.

EFFECTS OF VARIOUS PARAMETERS ON TOTAL OSCILLATING PRESSURES

Tip clearance.—Figure 6 illustrates the effect of tip clearance d on the free-space oscillating pressure distribution. As clearance is reduced for a given tip Mach number, pressures along a line parallel to the propeller axis tend to increase but the important change seems to occur in a region approximately one propeller radius wide in the vicinity of the plane of rotation. In this figure and in several succeeding ones the horizontal scale is x/D and denotes distances from the plane of rotation; positive values denote positions ahead of the propeller plane and negative values denote positions behind it.

Blade loading.—Figure 7 shows the extent to which the free-space pressure distribution may be changed, at a constant tip Mach number and clearance, by changing the blade

(a) Reinforced plywood wall (front view).

FIGURE 5.—Simulated fuselage walls used in tests.

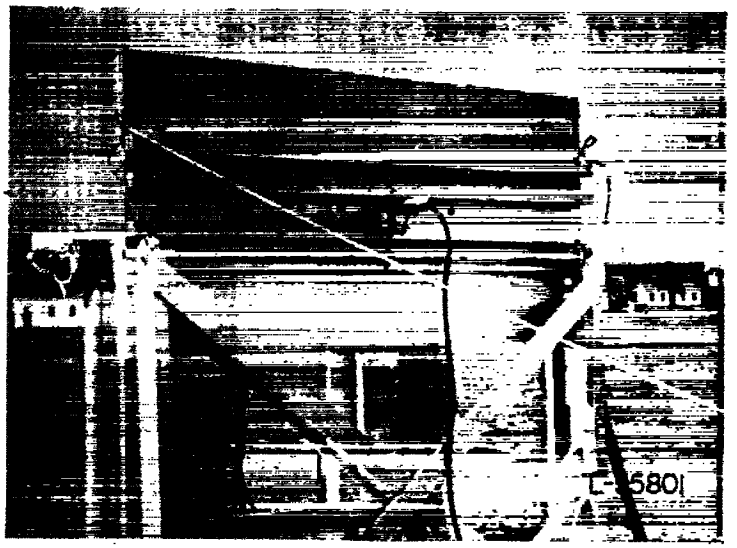

(b) Reinforced plywood wall (rear view) showing microphone support.

FIGURE 5.—Continued.

(c) Circular steel wall (side view with end stiffener removed) showing reinforcement and microphone supports.

FIGURE 5.—Concluded.

loading. When the pressure ordinate is plotted as the ratio $\bar{p}_c/C_P$, all data at a given tip Mach number can be compared on an equal power basis. Three different operating conditions are represented since at $\beta_{0.75}=8°$ the propeller is lightly loaded, at $\beta_{0.75}=15°$ it is heavily loaded but unstalled at the tips; whereas at $\beta_{0.75}=20°$ it is stalled. For the condition $\beta_{0.75}=20°$, the thrust component of pressure becomes of small importance relative to the torque component, and the pressure distribution tends to peak in the plane of rotation. For the unstalled condition where C_T is relatively large, the free-space pressures are a maximum at approximately ⅛ of a diameter ahead of and behind the plane of rotation.

Power coefficient.—In figure 8 some experimental free-space pressure coefficients $\bar{p}_c$ are plotted against power coefficient C_P for four different propellers and at two different tip Mach numbers. At a given tip Mach number the relation between $\bar{p}_c$ and C_P is seen to be approximately linear. A comparison between the total pressures produced by a two-blade and a four-blade propeller at equal power coefficients is given. As is indicated in figure 8, less pressure is produced by the four-blade propeller than by the two-blade propeller at the same power coefficient, although at tip Mach number 1.00 the differences are relatively small. Figure 8 shows that comparable data for the NACA 4–(5)(08)–03, the NACA 4–(3)(06.3)–06, and the Clark Y propeller are in good agreement. Blade plan form and solidity are thus not considered to be significant parameters. In addition, for a given M_t, C_P, and d/D, pressure coefficients for propellers of different diameter are shown to be approximately equal.

Tip shape.—The 3 two-blade propellers for which data are given in figure 8 differ in plan-form shape and in the shank sections, but all have rounded tips. Thus it is seen that the pressures produced are not affected very much by small differences at the inboard stations. Two-blade configurations of the NACA 4–(5)(08)–03 propeller and the square-tip propeller were tested to determine the effect of

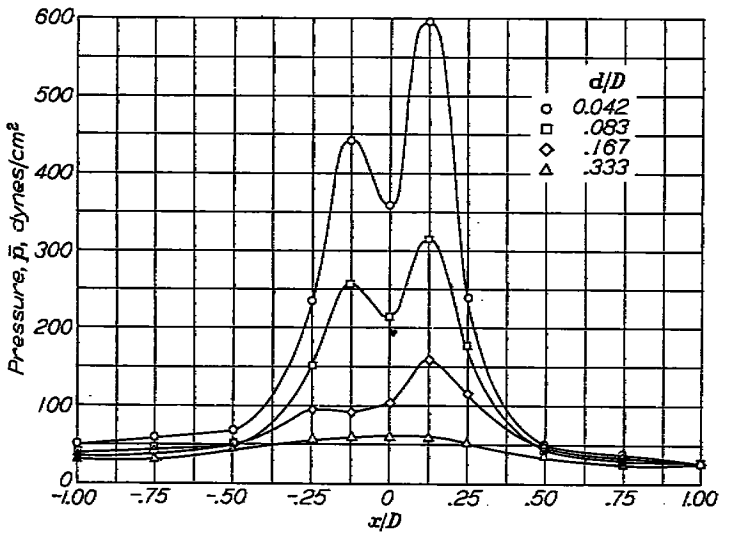

FIGURE 6.—Effect of tip clearance on the free-space pressures for NACA 4-(5)(08)–03 propeller. $B=4$; $\beta_{0.75}=10°$; $M_t=0.60$.

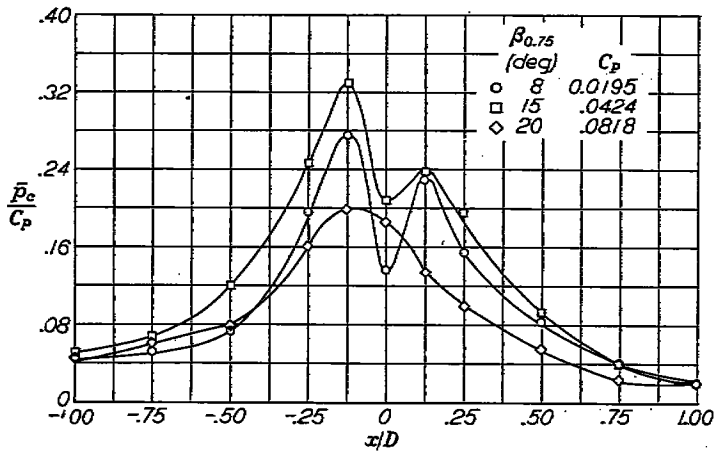

FIGURE 7.—Effect of blade loading on the free-space pressure distribution for NACA 4-(5)(08)–03 propeller. $B=2$; $M_t=0.60$; $\frac{d}{D}=0.083$.

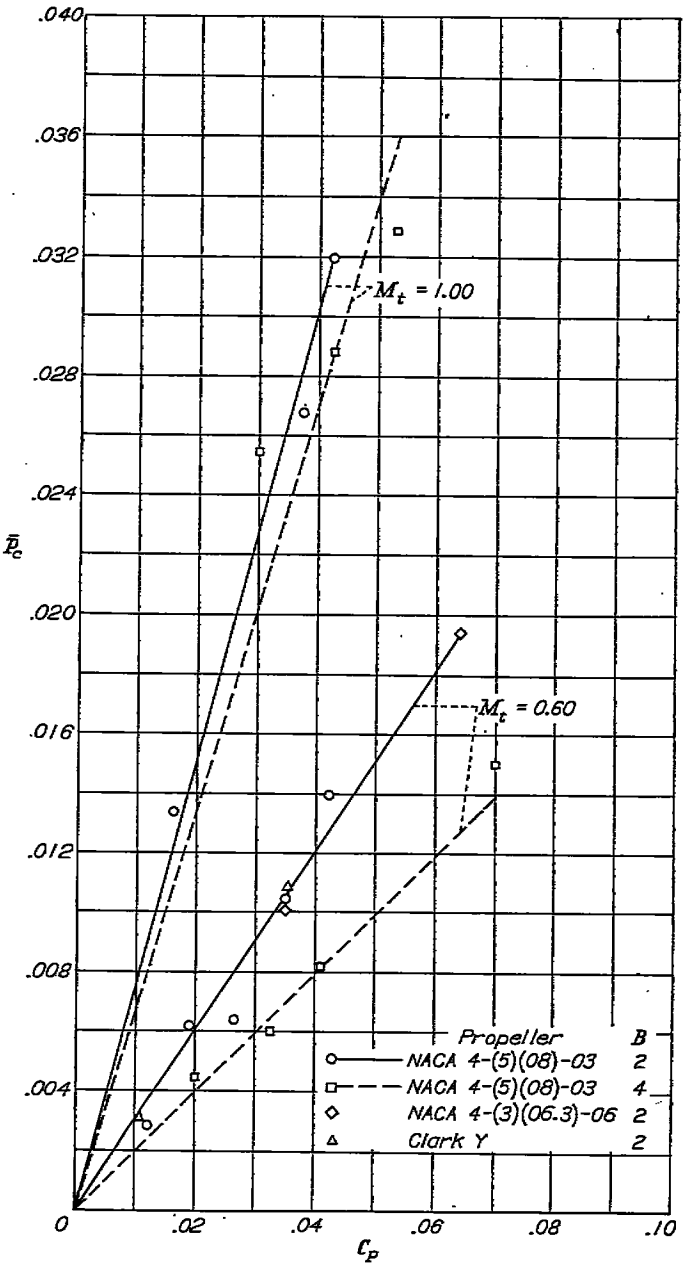

FIGURE 8.—Effect of power coefficient and tip Mach number on the oscillating-pressure coefficients of two- and four-blade propellers in the plane of rotation. $\frac{d}{D}=0.042$.

tip shape. These propellers have identical airfoil section, and the only essential difference in plan form is at the tips. Both propellers were tested at the same blade angle and tip speed and at approximately the same power to get comparable data. Results shown in figure 9 indicate that blade-tip shape is not a significant parameter.

Effect of reflecting surfaces.—In order to determine the effect that a reflecting surface has on the impinging pressures, tests were made with a flat vertical wall and a circular-shaped wall. These results are compared with corresponding free-space data in figure 10. Pressures measured in the plane of a flat vertical wall are seen to be approximately double the free-space values. Corresponding data for a circular wall indicate an increase over the free-space values, but this increase is somewhat less than that for the flat wall.

Comparison with full-scale data.—In order to compare these measurements with full-scale data some check points for the static condition were obtained from a test airplane. Since the full-scale propeller had three blades and operated at much larger power coefficients than the model propellers, no direct comparison could be made. The model data have been extrapolated to the larger power coefficients, however, and interpolations were made at the corresponding tip Mach numbers. The estimates thus obtained are given in the following table along with pertinent data from the full-scale tests for comparison:

M_t	Propeller diameter (ft)	Number of blades	Horsepower	C_P	d/D	$\bar{p}$, measured (dynes/cm²)	$\bar{p}$, extrapolated from model data (dynes/cm²)
0.49	12.92	3	466	0.129	0.083	350	420
.49	12.92	3	466	.129	.167	240	280
.70	12.92	3	1,500	.135	.083	1,500	1,440
.80	12.92	3	1,500	.135	.167	1,150	975

Thus it is seen that model data may be extrapolated to higher values of C_P with a fair amount of accuracy.

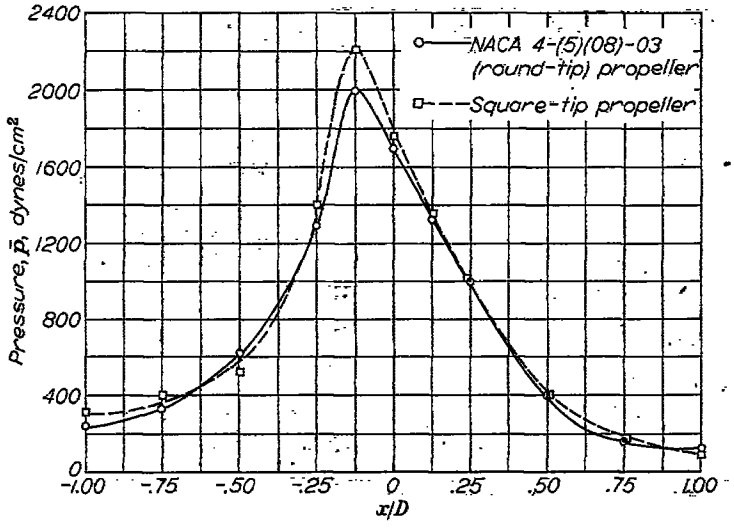

FIGURE 9.—Effect of propeller tip shape on the free-space pressures.

$B=2$; $\beta_{0.75}=15°$; $M_t=0.75$; $\frac{d}{D}=0.083$.

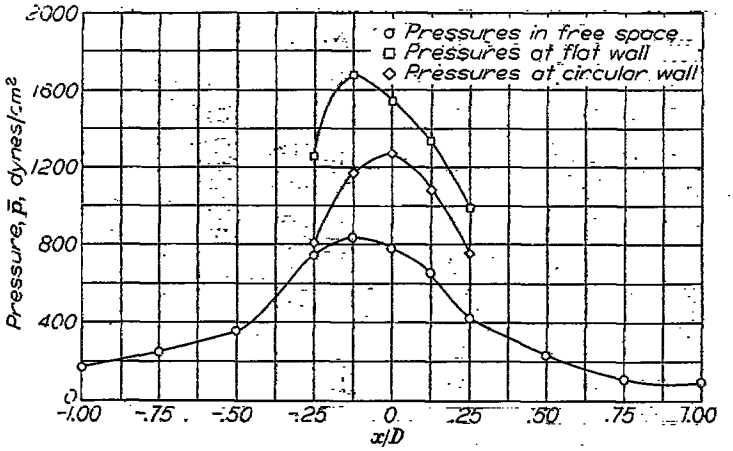

FIGURE 10.—Effect of reflecting surfaces in the pressure field of the NACA 4-(5)(08)-03 propeller. $B=2$; $\beta_{0.75}=20°$; $M_t=0.60$; $\frac{d}{D}=0.083$.

HARMONIC ANALYSES OF OSCILLATING PRESSURES

AMPLITUDES

Experiment.—Data presented thus far have shown the behavior of total oscillating pressures as measured in free space. The subsequent discussion illustrates the behavior of each of the first four harmonics of pressure for a two-blade propeller.

The effect of power coefficient on the relative amplitudes of the first four harmonics at three different tip Mach numbers in the plane of rotation $\left(\frac{x}{D}=0\right)$ is shown in figure 11. All harmonics are seen to follow a straight-line relationship between power coefficient C_P and pressure amplitude at $\frac{x}{D}=0$. Figure 11 (a) shows that, for the NACA 4-(5)(08)-03 two-blade propeller, the fundamental frequency is predominant at $M_t=0.75$ and each higher harmonic is smaller in amplitude. This order is completely reversed at $M_t=1.00$ as indicated in figure 11(c). At this speed the fundamental has the smallest amplitude, and the higher-order harmonics are progressively larger. At a tip Mach number of 0.90, as shown in figure 11(b), the amplitudes are more nearly equal which fact indicates that at this particular speed there is a transition between the two extremes shown in figures 11(a) and 11(c).

The "cross over" phenomenon shown in figure 11 for pressures in the plane of rotation does not seem to occur in the tip Mach number range of the tests where $\frac{x}{D}\neq 0$. At all points investigated outside of the plane of rotation the amplitude was found to decrease as the order of the harmonic increased. This result is shown in figure 12 where the harmonic amplitude variations for three different tip Mach numbers at several points in the pressure field are given.

Comparison of theory with experiment.—In the development of the theory the pressures at a point in space due to the forces distributed over the propeller disk are given by a double integration. The first integration is around the blade path from $\theta=0$ to $\theta=2\pi$ and the second integration is along the blade radius from $r=0$ to $r=R$. For simplification

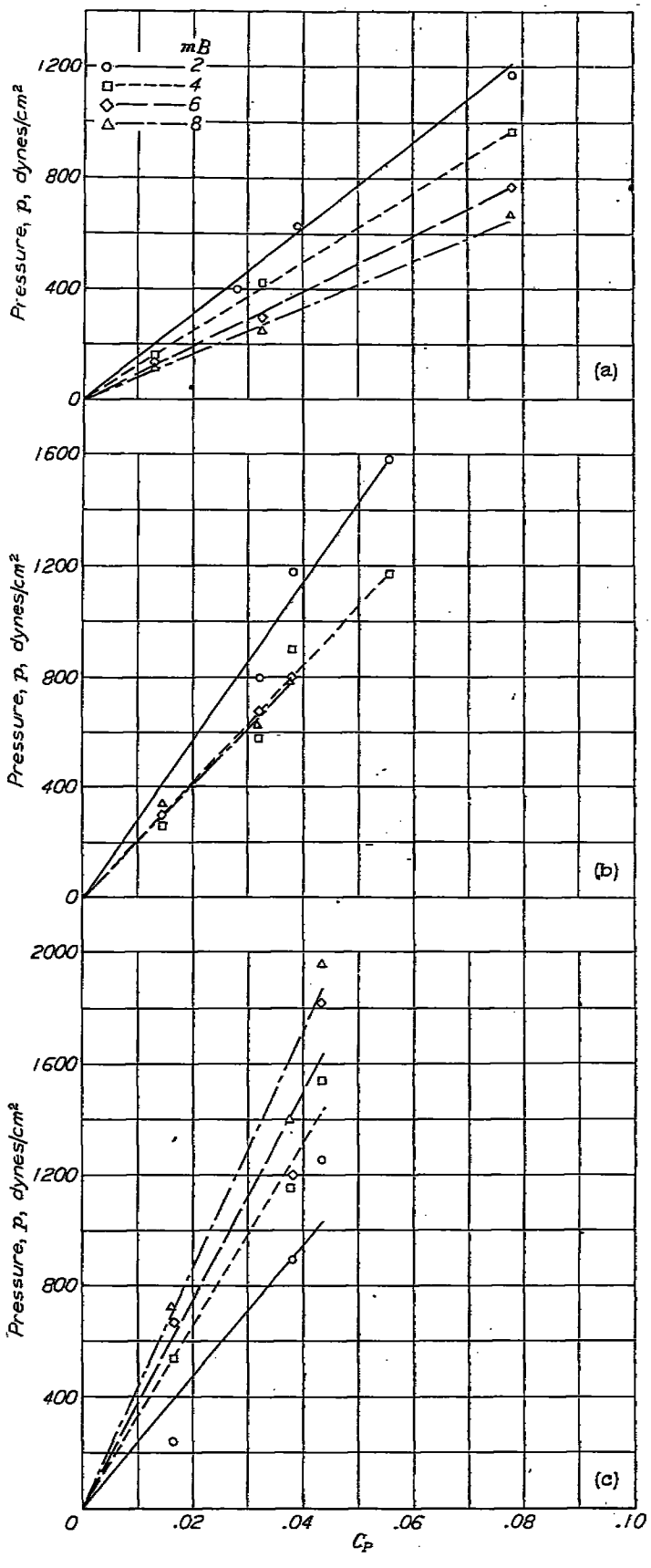

(a) M_t=0.75.
(b) M_t=0.90.
(c) M_t=1.00.

FIGURE 11.—Effect of power coefficient on the relative pressure amplitudes of the first four harmonics of the NACA 4-(5)(08)-03 two-blade propeller in the plane of rotation. $\frac{d}{D}$=0.083.

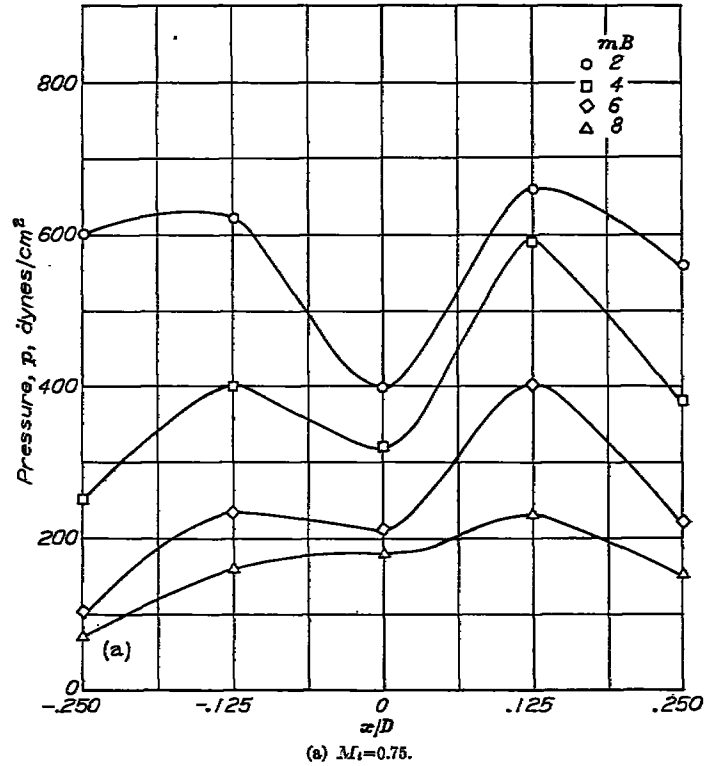

(a) M_t=0.75.

FIGURE 12.—Relative amplitudes of four harmonics of NACA 4-(5)(08)-03 propeller. B=2; $\beta_{0.75}$=10°; $\frac{d}{D}$=0.083.

the second integration is eliminated and all forces on the propeller disk are assumed to be concentrated at an effective radius. This effective radius R_e is a function of the blade thrust distribution and torque distribution and the manner in which the forces at each blade element contribute to the free-space pressures at a point in space for a given harmonic. Thus R_e may differ for the various harmonics and may be different for the thrust and torque terms of equation (2).

The effective radius for a given harmonic was evaluated herein by comparing the calculations with corresponding experimental values. The calculated curves were based on values of x/D corresponding to those shown for the experimental data. Calculations in figure 13(a) for R_e=0.8R give good agreement with experiment for the propeller operating at $\beta_{0.75}$=15° and M_t=0.75. Similar calculations for this propeller at $\beta_{0.75}$=10° and M_t=1.00 and for R_e=0.8R overestimate the maximum oscillating pressures. (See fig. 13(b).)

In figure 14 the experimental and calculated pressures at $\frac{x}{D}$=−0.125 are compared for the first three harmonics of the NACA 4-(5)(08)-03 two-blade propeller at $\beta_{0.75}$=10°. The calculated points were obtained by using equation (2) and the thrust and torque coefficients listed in the figure. Equation (2) predicts pressures over the entire test range of tip Mach numbers with the same amount of accuracy. The deviation then appears to be essentially due to blade loading and not due to tip Mach number. The use of R_e=0.8R in this case resulted in overestimating all pressures by about 40 percent.

For conditions of figure 14 a variation of R_e in equation (2) resulted in a nearly uniform change in pressure amplitude for the fundamental frequency of a two-blade propeller throughout the given tip Mach number range. Figure 15 shows the amount of this variation for three values of R_e at $\frac{x}{D}=-0.125$. For these conditions calculations for $R_e=0.7R$ most nearly duplicated the experimental results. Thus it may be seen that the maximum pressures which usually occur at $\frac{x}{D}=-0.125$ may be predicted by using an effective radius varying from $0.7R$ to $0.8R$ for the propeller in these tests. This propeller is believed to be representative of high-speed propellers. Since propellers are normally operated through a wide range of loading conditions, a value of R_e which will be valid for the extreme case is considered most useful. For this particular propeller $R_e=0.8R$ is recommended to give conservative calculated pressures.

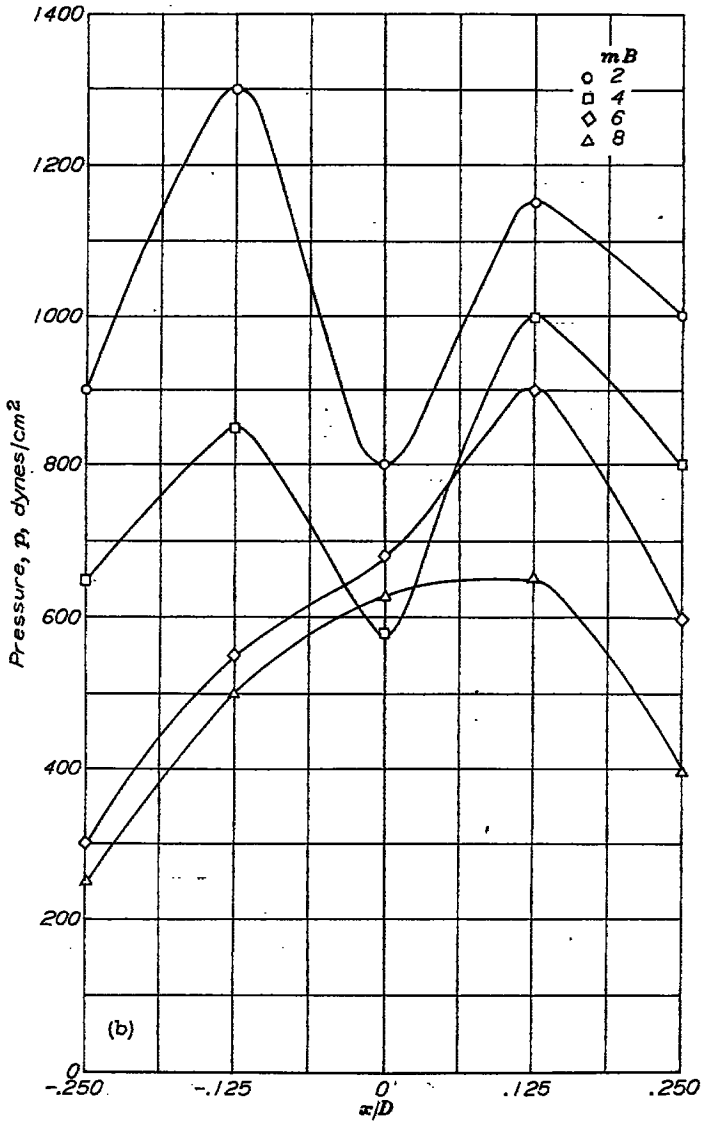

(b) $M_t=0.90$.

FIGURE 12.—Continued.

The data of figure 7 indicate that the ratio of pressure coefficient to power coefficient is lower for the lightly loaded and the stalled propeller than for the heavily loaded propeller. Thus, since the value of $R_e=0.8R$ will adequately predict the pressures for a heavily loaded propeller, it will tend to overestimate the pressures at other operating conditions.

Deming in reference 2 shows that for a propeller at a given blade angle the sound pressures at a distance vary approximately as the powers of the tip speed of 5, 6.5, and 8 for mB values of 2, 4, and 6, respectively. Since the power varies approximately as the cube of the tip speed, the sound

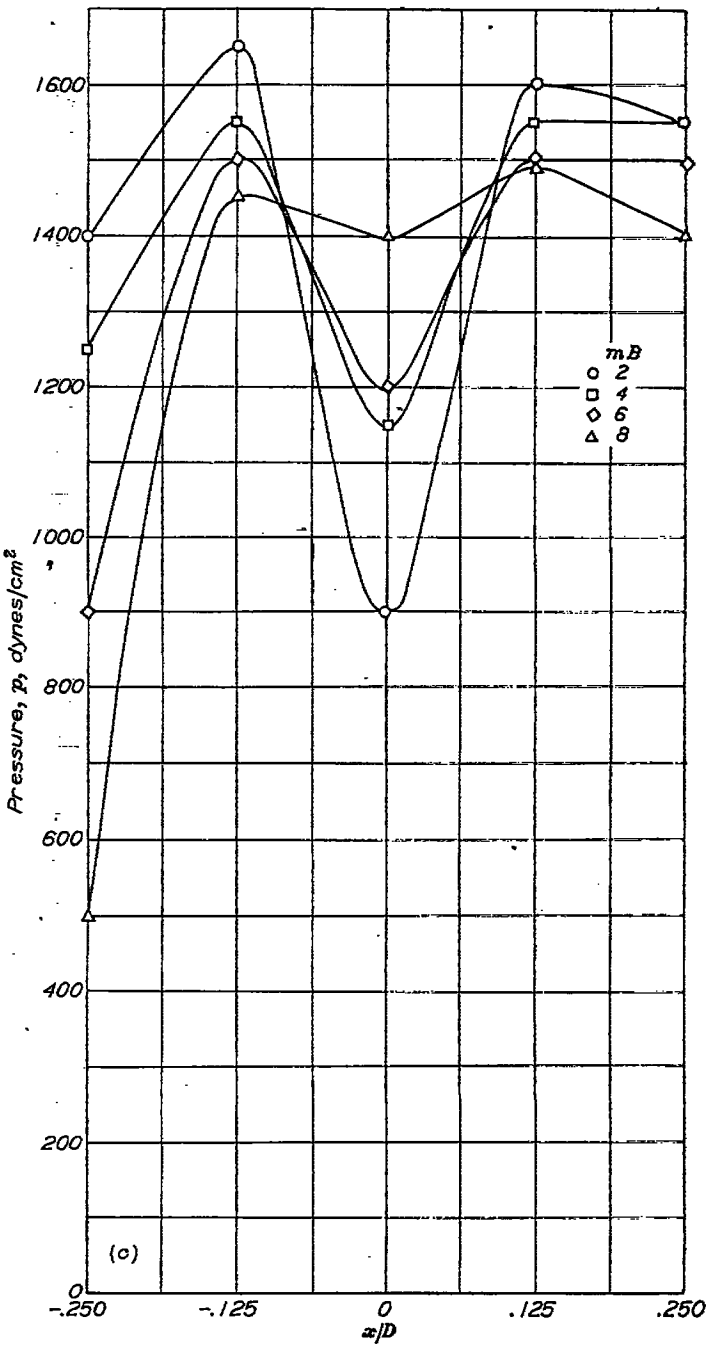

(c) $M_t=1.00$.

FIGURE 12.—Concluded.

pressure at constant power may be seen to vary as the powers of the tip speed of 2, 3.5, and 5 for $mB=2$, 4, and 6, respectively. At a distance then, an increase in tip speed at constant power results in an increase of sound pressure for all harmonics. This condition does not exist for all harmonics, however, in the region near the propeller. Figure 14 (a) shows that for a given blade angle the pressures varied considerably less with tip speed than was observed in reference 2. In figure 16 the experimental data of figure 14 (a) is plotted to show the effect of tip Mach number at constant power on the free-space pressures of each harmonic. For these conditions the pressure per unit power is decreased as the tip Mach number is increased for $mB=2$, whereas for $mB=6$ the trend seems to reverse. The pressure amplitude for $mB=4$ seems to be essentially independent of tip Mach number.

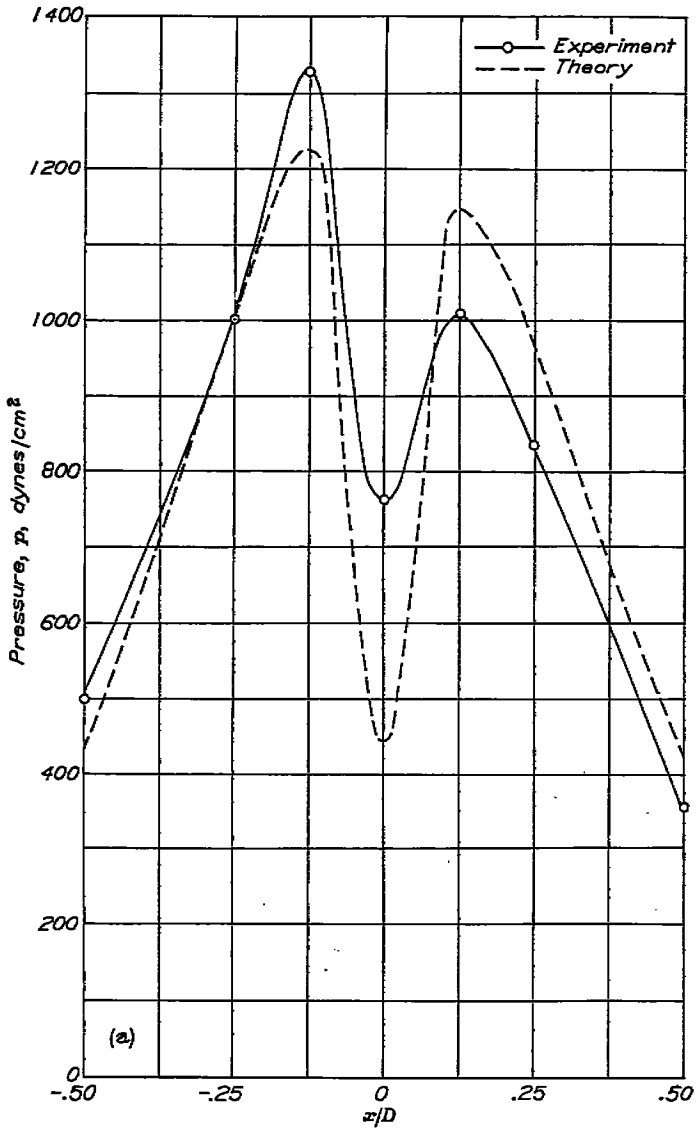

(a) $M_t=0.75$; $\beta_{0.7R}=15°$.

FIGURE 13.—Free space pressure distribution of the first harmonic o the NACA 4-(5)(08)-03 propeller. $B=2$; $\frac{d}{D}=0.063$; $R_s=0.8R$.

Calculations in the plane of rotation for the pressure amplitude of the fundamental of a two-blade propeller have been made by means of Gutin's simplified equation and also by equation (2) of the present report. The results obtained by using the two methods are plotted as a ratio against d/D in figure 17 for tip Mach numbers of 0.75 and 1.00. The Gutin equation is seen to underestimate the pressures at low d/D values. At a given d/D value the order of agreement of the two methods is seen to change with tip Mach number and also may be different for each harmonic and at other points in space. These results would preclude the use of Gutin's simplified equation with a convenient adjustment factor since the adjustment factor would probably be different in every case.

PHASE RELATIONS

The fuselage-wall designer should know not only the relative amplitudes of the harmonics of pressure produced by the propeller but also something of the phase relations. Equation (1) will predict the phase between the impinging pressures of any given harmonic at two different points in space.

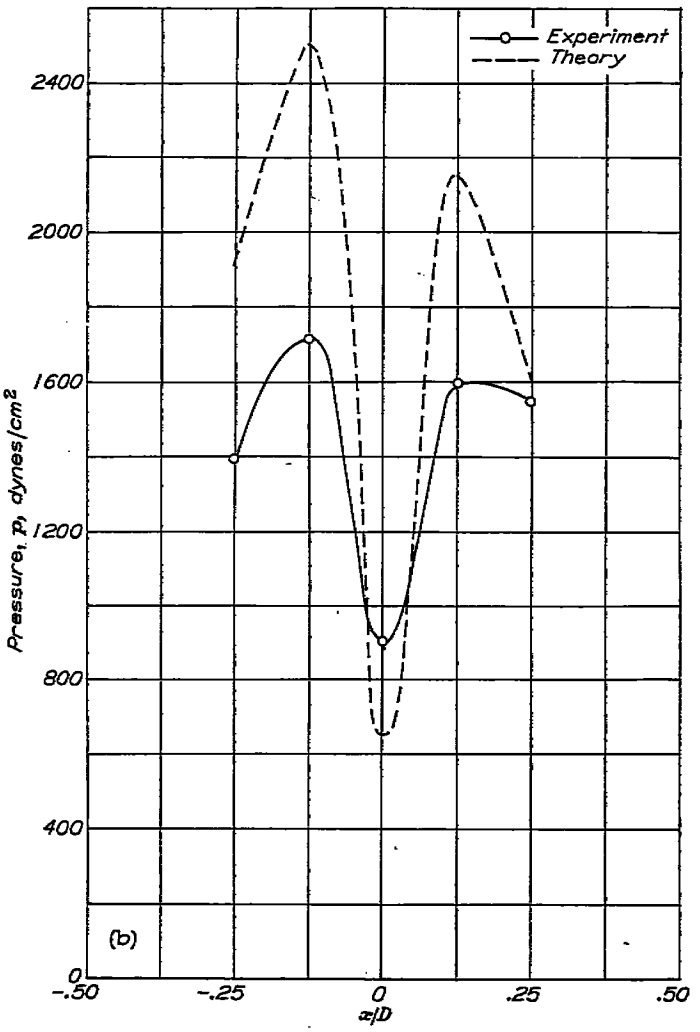

(b) $M_t=1.00$; $\beta_{0.7R}=10°$.

FIGURE 13.—Concluded.

The phase may also be predicted by use of equation (2). For given conditions equation (2) gives the pressure at a point in space as the product of a constant term and the square root of the sum of the squares of the real and imaginary components which are, respectively, the first and last terms within the large parentheses. If the algebraic values of each of these terms are known, the phase relations may be easily determined.

By this method calculations of the pressures produced simultaneously by the fundamental frequency at two points in space, equidistant ahead of and behind the propeller plane and for a tip Mach number of 0.75, gave a phase difference of 165°. Comparative measurements at these same operating conditions gave a corresponding value of 155°; thus, the validity of equation (2) is further verified. Similar calculations for the same propeller at the same tip speed but for a larger blade-angle setting gave a phase difference of 125°. A comparison of these results indicates that the phase angle between the pressures ahead of and behind the propeller plane tends to decrease in magnitude as C_Q increases with respect to C_T.

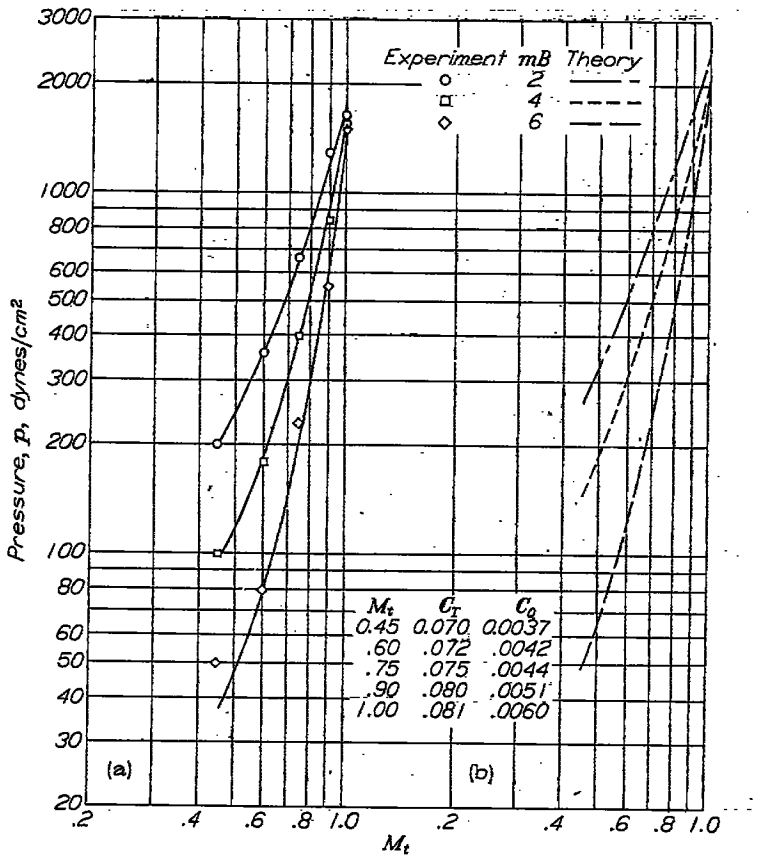

(a) Experiment. (b) Theory. R_e=0.8R.

FIGURE 14.—Effect of tip Mach number on pressure amplitude of the first three harmonics for NACA 4-(5)(08)-03 propeller. B=2; $\beta_{0.75}$=10°; $\frac{x}{D}$=−0.125; $\frac{d}{D}$=0.083.

Figure 18 shows the total-pressure wave forms as recorded at three different points in space for five different tip Mach numbers. These are Du Mont dual-beam cathode-ray oscillograph pictures of the microphone voltage output, which is the upper trace, and a timing line of 300 cycles per second. The small vertical line on the timing line indicates the time at which the propeller blade passes through the xy-plane and is closest to the microphone. The line tracing the pressure indicates positive pressure when it moves downward and negative pressure when it moves upward, and time increases from left to right. The photographs taken at a tip Mach number of 1.00 indicate a relatively large contribution by the higher harmonics, whereas at the lower tip Mach numbers the low harmonics are clearly predominant. Figure 18 is included primarily for information in case a more detailed analysis of these wave forms is desired.

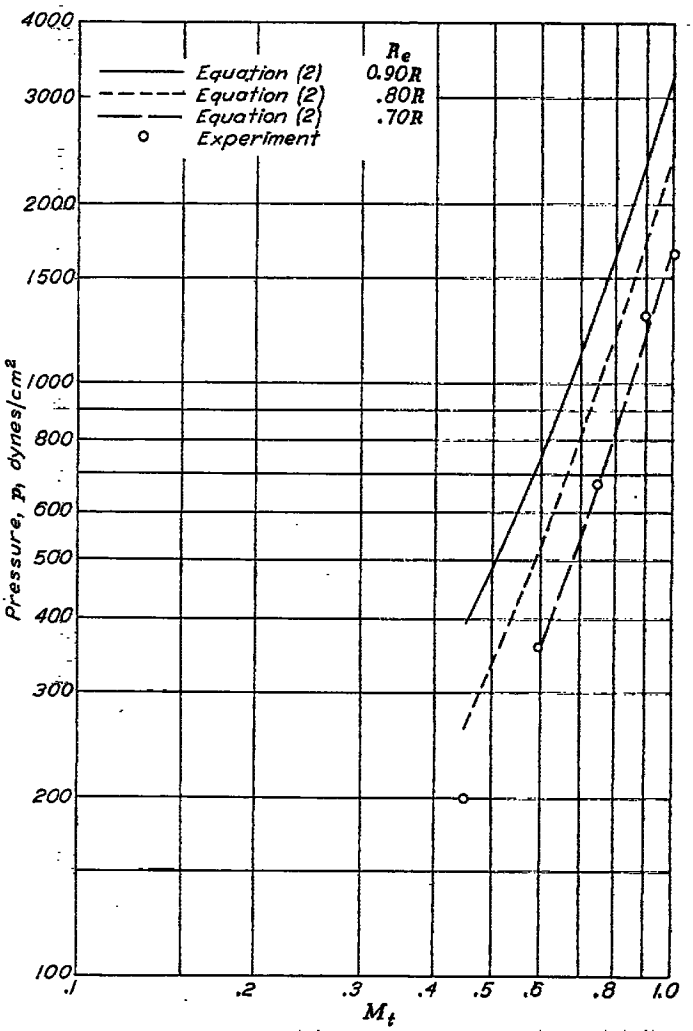

FIGURE 15.—Effect of tip Mach number and effective radius on pressure amplitude of the first harmonic for NACA 4-(5)(08)-03 propeller. B=2; $\beta_{0.75}$=10°; $\frac{x}{D}$=−0.125; $\frac{d}{D}$=0.083.

CHARTS FOR ESTIMATING FREE-SPACE PRESSURES

The theory given in this report is adequate for predicting free-space oscillating pressures for any static condition. The complexity of the method, however, makes it desirable to provide a more convenient means of estimating these pressures. The charts of figure 19 are presented for this purpose. In contrast to the analytical method these charts do not predict the pressures at a given point but instead give a first approximation of the maximum free-space pressure coefficients of a given harmonic near the plane of rotation of the propeller. This information may be determined easily from the appropriate chart, provided that the power coefficient, tip Mach number, and tip clearance are known for a given propeller.

The charts are based on data for unstalled conditions and the pressures involved were determined by averaging the maximum values measured in front of and behind the plane of rotation at each test condition. These maximum values usually occurred at $\frac{x}{D}=\pm 0.125$. The free-space pressure coefficients thus obtained were found to vary approximately linearly with power coefficient as do those measured in the plane of rotation. (See fig. 11.) Thus the thrust terms are neglected and the charts are based on power coefficients of the tests. The charts may be used, however, for power coefficients larger than those for which data were taken. The charts are based primarily on experimental measurements at $\frac{d}{D}=0.083$ and on a sufficient number of measurements at other d/D values to establish the attenuation curve in figure 20. This curve was faired from a composite plot of data which were adjusted to equal magnitudes at $\frac{d}{D}=0.083$.

Charts for values of mB of 2, 3, 4, 5, 6, and 8 were determined by faired data from two-blade and four-blade propellers. In equation (2) where m and B always appear as a product, the second harmonic of a two-blade propeller has the same strength as the fundamental of a four-blade propeller for the same operating conditions. Because of this fact, which has also been confirmed experimentally, and because the fundamental frequency has been found to be predominant in this critical region of maximum pressures, the charts are useful for estimating pressures produced by the fundamental frequencies of propellers which have from two to eight blades; they may also be used to predict the pressures of harmonics in the range of values of mB from 2 to 8.

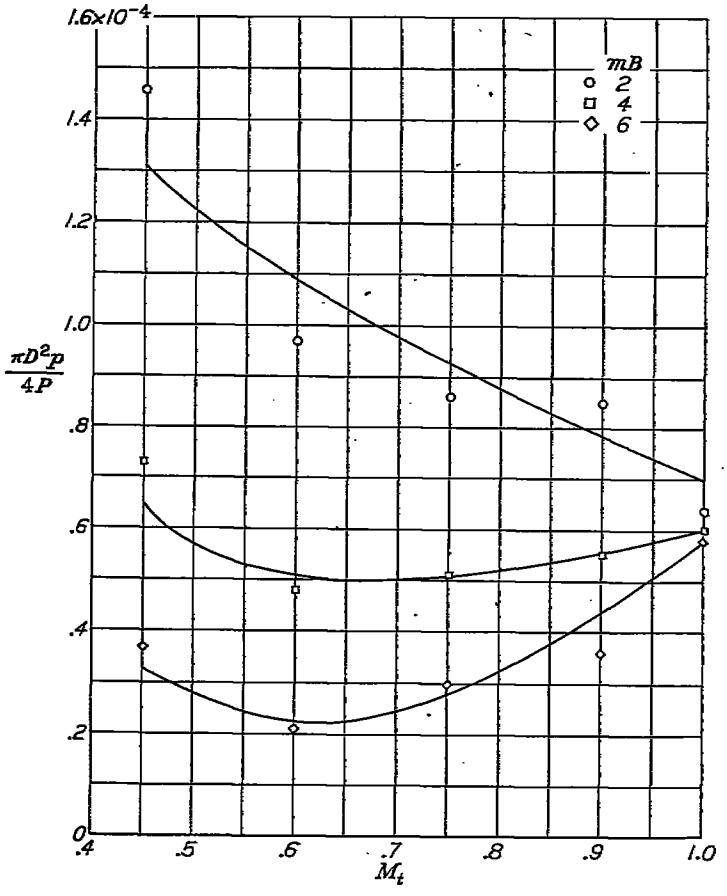

FIGURE 16.—Free-space oscillating pressure divided by power per unit disk area as a function of tip Mach number. NACA 4-(5)(08)-03 propeller. $B=2$; $\beta_{0.75}=10°$; $\frac{x}{D}=-0.125$; $\frac{d}{D}=0.083$.

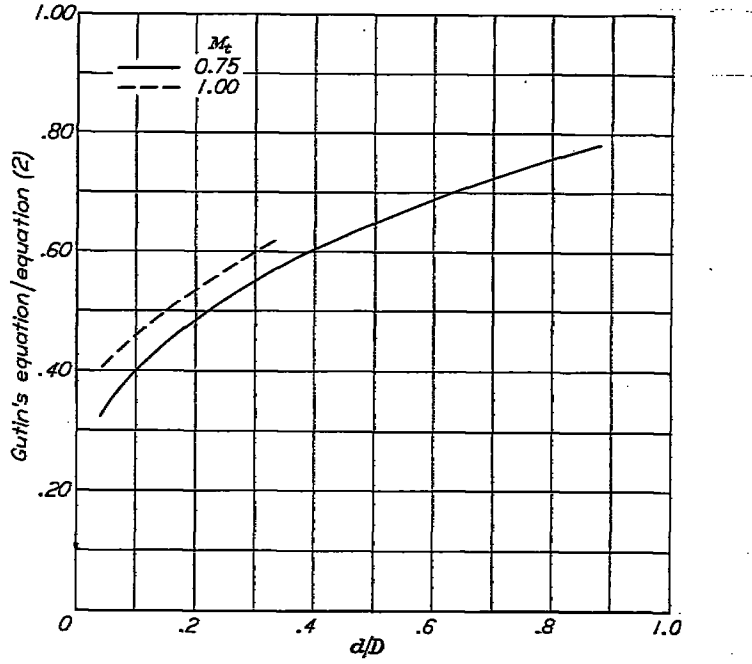

FIGURE 17.—Comparison of Gutin's simplified solution with equation (2) for the fundamental frequency of a two-blade propeller in the plane of rotation.

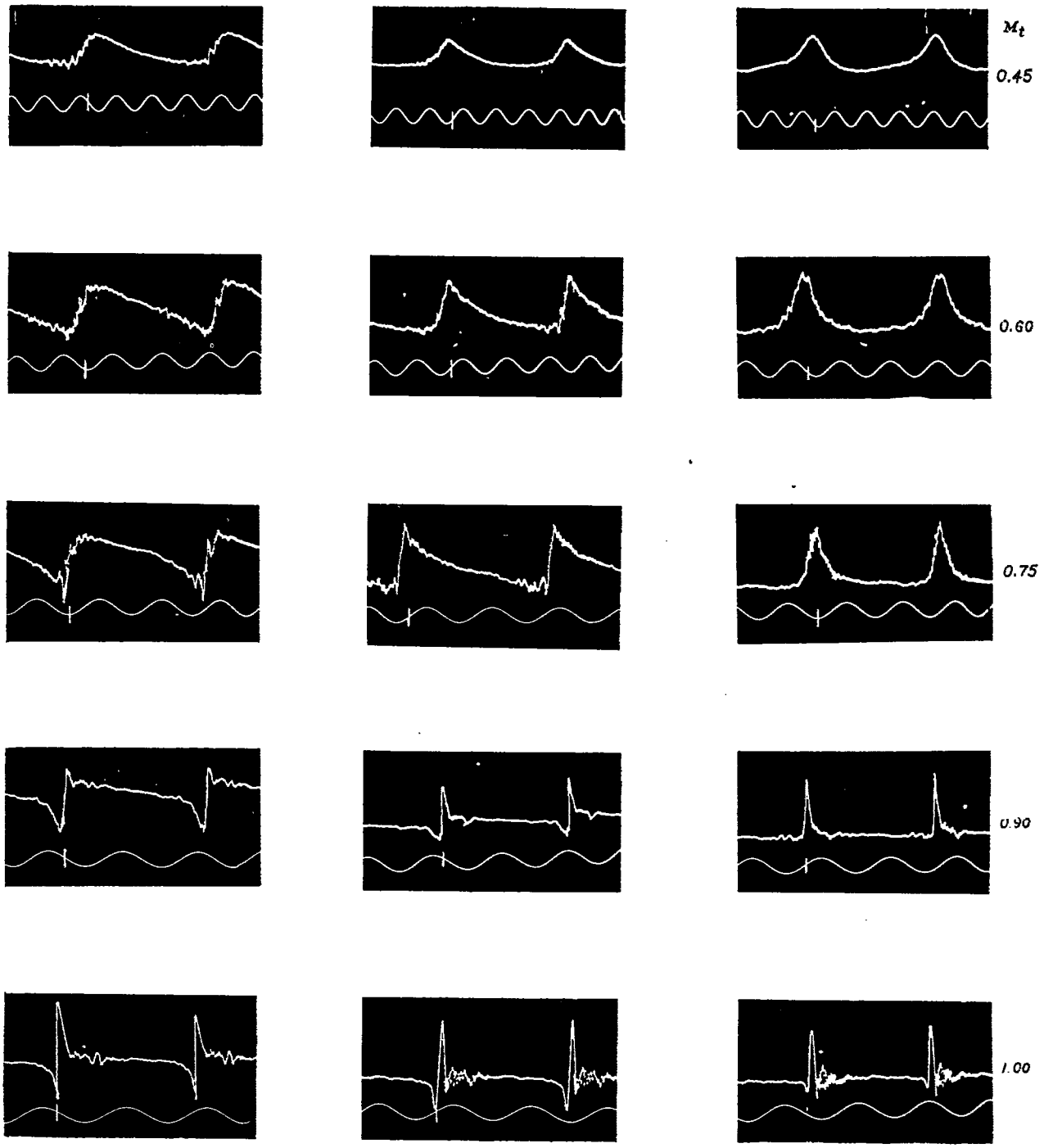

(a) $\frac{x}{D}=-0.125$. (b) $\frac{x}{D}=0$. (c) $\frac{x}{D}=0.125$.

FIGURE 18.—Effect of tip Mach number on the pressure wave forms at three different points in space for NACA 4-(5)(08)-03 propeller. $B=2$; $\beta_{0.75}=12°$; $\frac{d}{D}=0.167$. (Bottom trace in each photograph is 300-cps timing line.)

950646—51——52

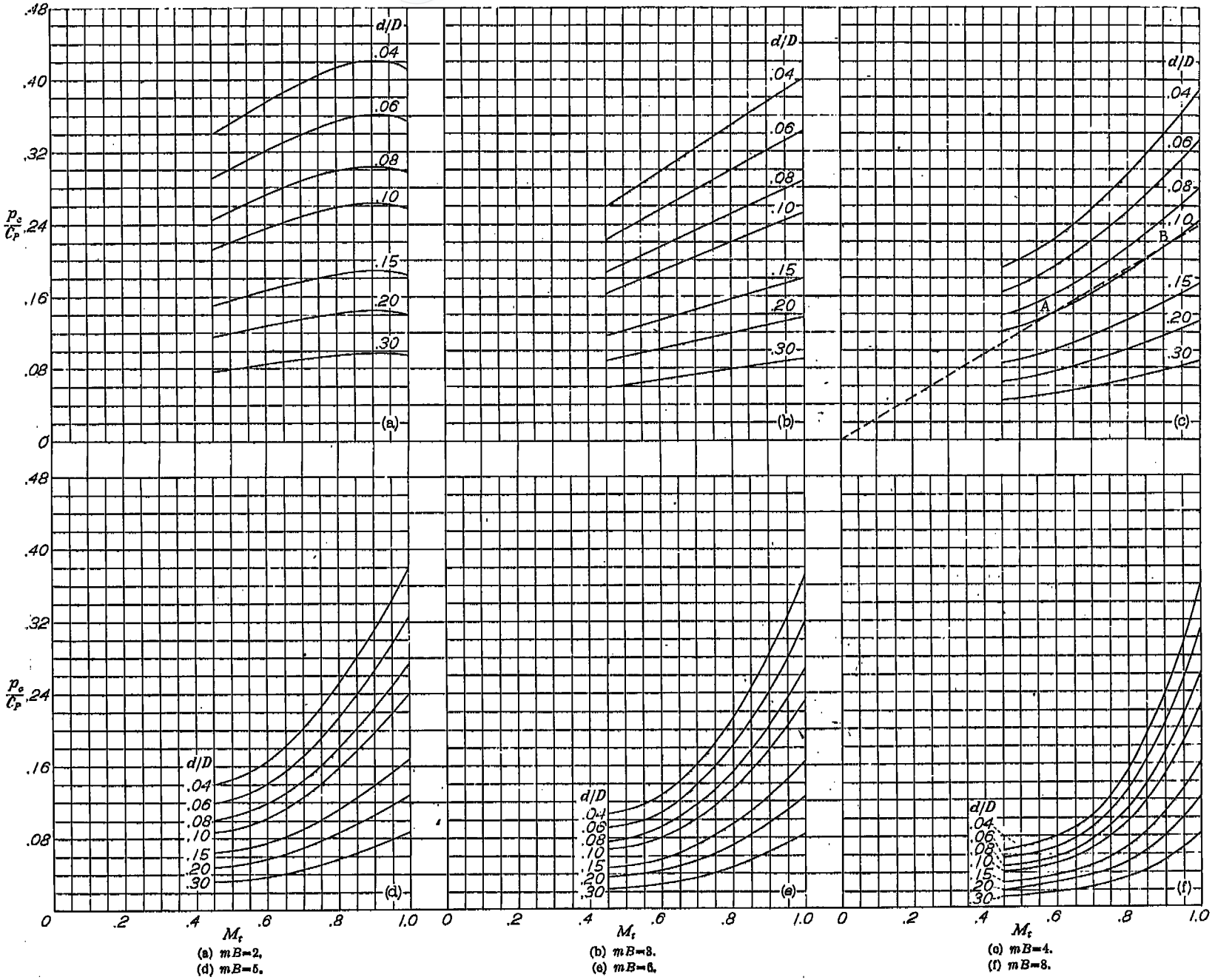

(a) $mB=2$, (b) $mB=3$, (c) $mB=4$,
(d) $mB=5$. (e) $mB=6$. (f) $mB=8$.

FIGURE 19.—Charts for estimating the maximum free-space pressures near the plane of rotation of a rotating propeller.

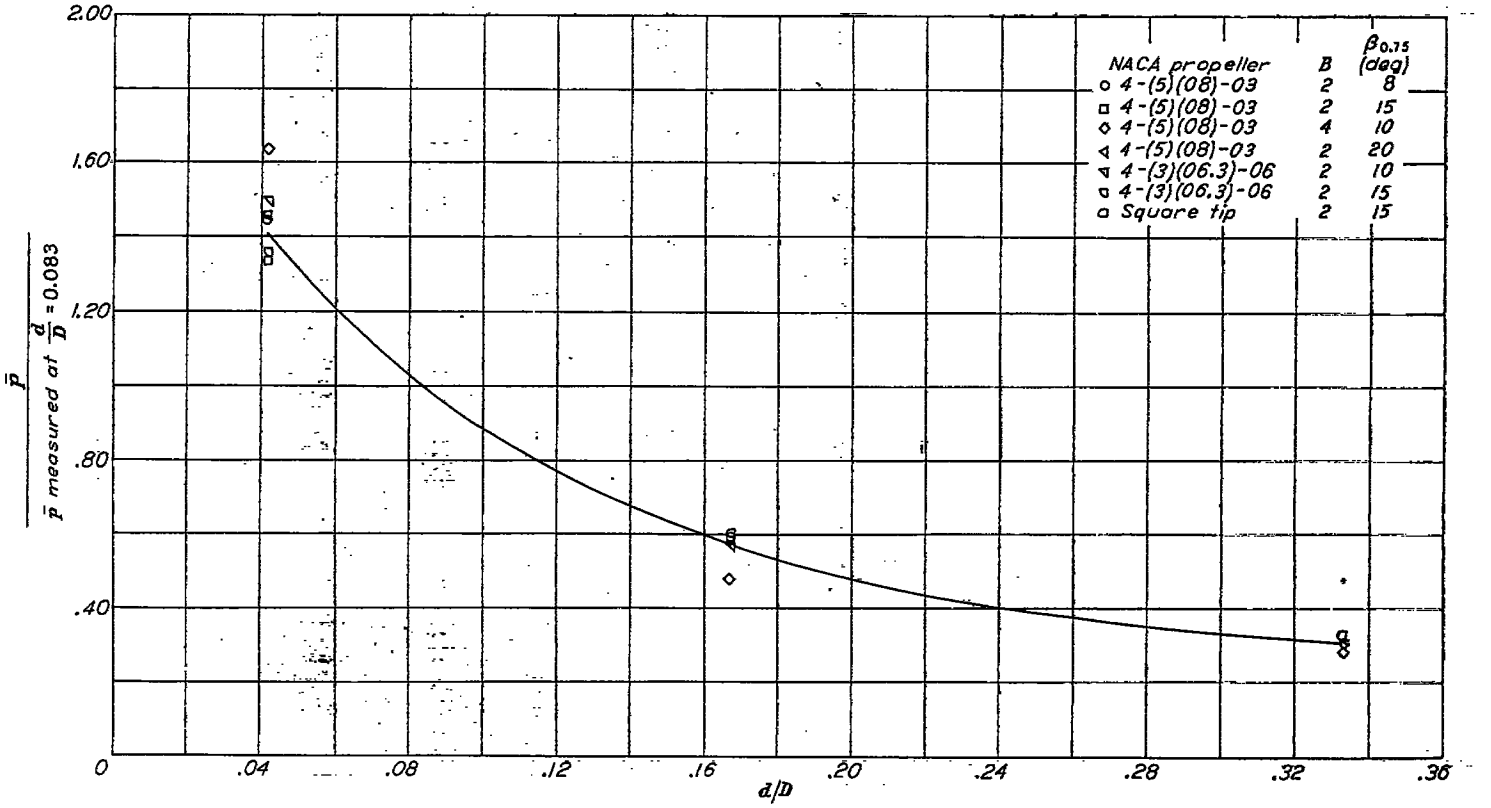

FIGURE 20.—Free-space pressure attenuation curve used in calculating the values of figure 19.

As first illustrated in figure 12, the charts show in general that at tip Mach number 1.00 all harmonics have very nearly the same maximum amplitude for comparable operating conditions, whereas at the lower tip Mach numbers the lower-order harmonics are predominant.

The effect of tip Mach number on the oscillating pressures for a propeller operating at constant power may be estimated from the relation of p_c, C_P, and M_t in the following manner. Since $p_c=\frac{p}{\rho n^2 D^2}$, $C_P=\frac{P}{\rho n^3 D^5}$, and $M_t=\frac{\pi n D}{c}$,

$$\frac{p}{P}=\frac{\pi}{c}\frac{p_c}{C_P M_t D^2}$$

or

$$\frac{p}{P\left/\left(\frac{\pi D^2}{4}\right)\right.}=\frac{\pi^2}{4c}\frac{p_c}{C_P M_t}$$

Thus in the charts of figure 19, lines of constant oscillating pressure per unit propeller power are straight radial lines through the origin. If the slope of the p_c/C_P curve at a given point is greater than the slope of a straight line from that point to the origin as at point B in figure 19 (c), the oscillating pressure will increase with an increase in tip Mach number for a constant power. If on the other hand the slope of the p_c/C_P curve at a given point is less than the slope of the straight line to the origin as at point A in figure 19 (c), the free-space pressure will decrease with increasing tip Mach number.

In general the charts of figure 19 show that at the low values of mB, the p_c/C_P curves are relatively flat and the oscillating pressures will decrease with increasing tip Mach number at constant power. For the higher mB values the reverse is true. This effect has already been indicated in figure 16 and is further shown in figure 21 where the ratio $p_c/C_P M_t$, which is proportional to the oscillating pressures per unit propeller power, is plotted for various values of mB as a function of tip Mach number. Data in figure 21 are faired data taken from the charts of figure 19.

Figure 21 shows that for values of mB less than 4 the oscillating pressure per unit power decreases with increased tip Mach number. The conclusion may be drawn that the pressure due to the fundamental mode of excitation for a four-blade propeller is essentially independent of tip Mach number when the power is held constant. Hence changing the tip Mach number will not materially affect the primary modes of fuselage vibration. It may be noted, however, that the large increase in pressure amplitude of the higher harmonics with increase in tip Mach number will greatly increase the noise levels in the fuselage.

FUSELAGE RESPONSE TO OSCILLATING PRESSURES

VIBRATION

Theory and experiments have been discussed which make possible the prediction of the oscillating pressures acting on the fuselage. The present section deals with the fuselage response to these pressures and indicates some of the factors

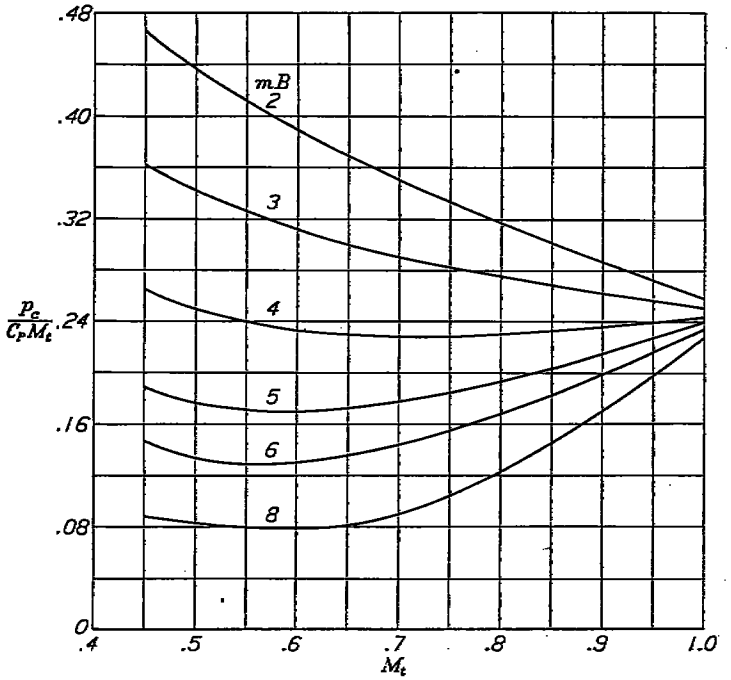

FIGURE 21.—Effect of tip Mach number at constant power on the pressure amplitudes of the fundamental frequencies of various propellers. $\frac{d}{D}$=0.10.

to be considered in solving the problem of fuselage vibration and noise. Since references 3 and 4 consider in detail the acoustical treatment for aircraft fuselages, no experiments were made on soundproofing. Some amplitude and frequency measurements, however, were made on vibration of two panels which were subjected to pressure impulses from propellers.

Experimental data.—The test panels were designed primarily as reflectors and were not intended for use in vibration studies. Thus, heavy construction was used in order to minimize the effect of panel vibration on the pressure measurements. The panel weights were approximately 8 pounds per square foot for the flat wall and approximately 5.5 pounds per square foot for the circular wall. These weights are appreciably greater than the normal fuselage weight of about 1 pound per square foot. Despite these weight differences the vibration data taken during the course of these tests are of interest in that they indicate the way in which the vibration amplitudes are affected by panel resonances.

Figure 22 (a) gives the vibration response of the flat wooden panel at the position of greatest vibration amplitude both before and after reinforcing. As a result of excitation by a two-blade propeller a resonance peak occurred at 130 cycles per second. Reinforcing the panel removed the resonant condition from the operating range. The response curve for the circular steel panel (fig. 22 (b)) shows a narrow resonance peak at 107 cycles per second. The steel shell has a more narrow frequency response than the wooden panel and thus indicates less damping. The peak amplitude of the circular wall is less than that for the flat wall even though the flat wall had more damping. Thus it is indicated that pressures on the circular wall are less than those on the flat wall. This condition is further indicated by the curves for the reinforced walls, because the flat wall has about twice the amplitude of the circular shell. Figures 22 (a) and 22 (b) indicate the necessity of removing any large wall resonances from the operating range. They also indicate that a curved wall has less vibration amplitude than a flat wall for comparable tip clearance and operating conditions.

Response of the reinforced flat wooden panel to excitation by a four-blade propeller, which absorbs slightly less power than the two-blade propeller of figures 22 (a) and 22 (b), is shown in figure 22 (c). A number of small resonance peaks appear in this figure; however, the over-all value of the amplitude is considerably less than for the two-blade propeller. Even though the pressures associated with the four-blade propeller at high tip Mach numbers will be nearly equal in amplitude to those for a two-blade propeller, the corresponding wall vibration amplitudes may be much smaller. This reduction is attributable to the greater wall inertia at the higher frequencies produced by the four-blade propeller.

Comparison of experimental data with theory.—A body such as a fuselage has an infinite number of vibration modes. The determination of the response to a forced vibration load such as a sound wave would require the vector summation of all the responses to the particular sound wave. Such a procedure is difficult, if not impossible. It has been found experimentally that at a particular exciting frequency the response of a body is predominantly determined by the vibration mode which is near the exciting frequencies. If the excitation is far from a resonant condition the amplitude of vibration may be estimated by considering only the inertia or mass of the panel. (See p. 219, reference 5.) As a first approximation, the natural frequency of the panel may be assumed to be zero and the material damping and radiation resistance may be neglected. Under such assumptions, the response of a panel to an oscillating force may be simply calculated as (p. 62, reference 6)

$$\xi_{02}=\frac{p_s}{M\omega_1^2} \qquad (3)$$

where ξ_{02} is the displacement from each side of the neutral position, p_s is the pressure measured at the panel surface, M is the mass of panel per unit area, and ω_1 is the angular frequency of sound in radians per second. Calculations of the vibration amplitudes of the test panels for the fundamental propeller frequencies have been made by equation (3) and are plotted in figure 22. The maximum pressures measured for the first harmonic near the plane of rotation and corrected for wall reflection were used in these calculations. Wall pressures used were 2 times free-space values for the flat surface and 1.5 times free-space values for the curved surface, as indicated by results given in figure 10. Total amplitude is $2\xi_{02}$. The calculated values are seen to be in good agreement with the vibration amplitudes measured for the reinforced panel except where resonant peaks occur (fig. 22).

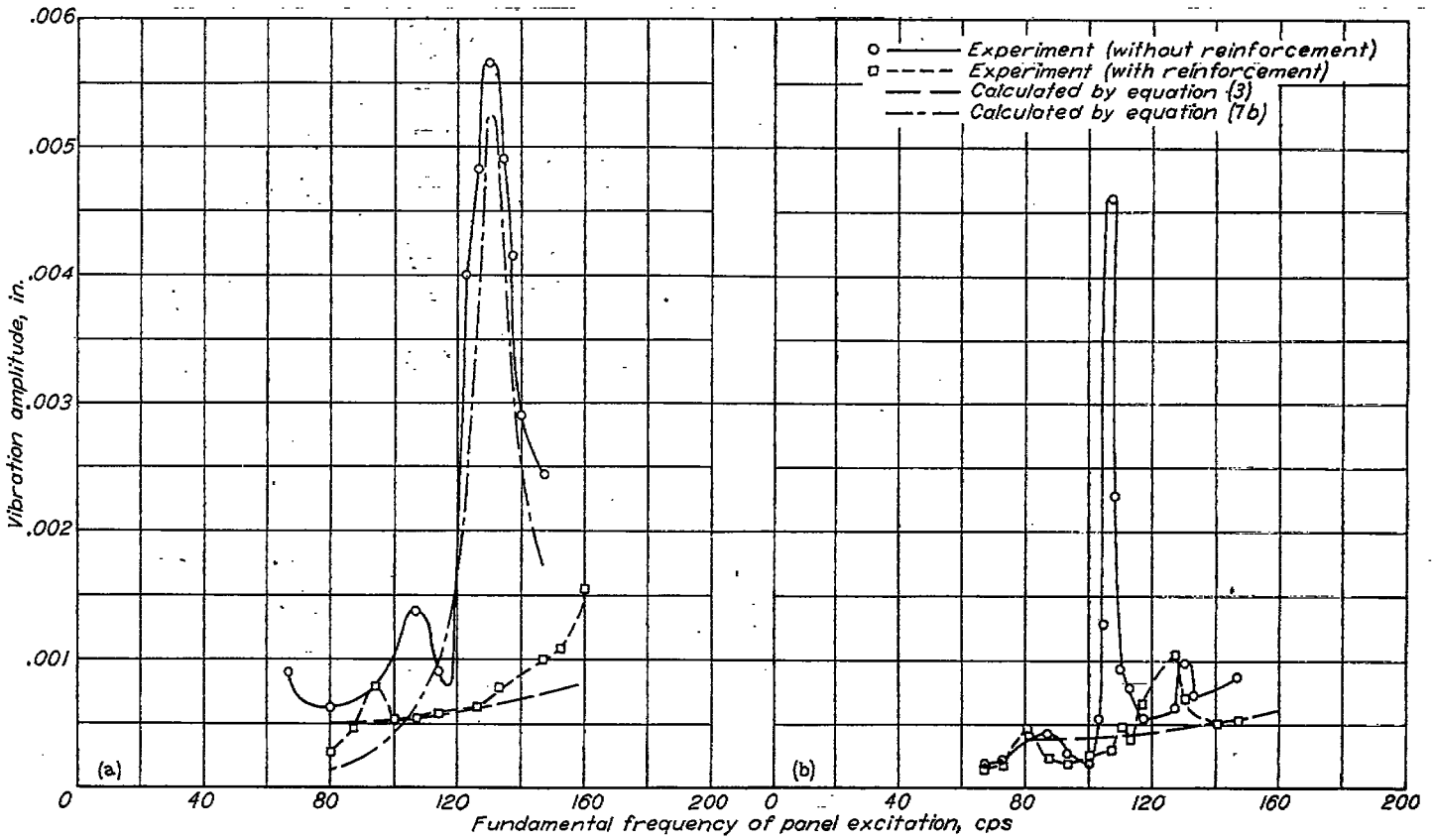

(a) Flat vertical wooden wall with two-blade propeller. (b) Circular steel wall with two-blade propeller.

FIGURE 22.—Panel frequency-response curves.

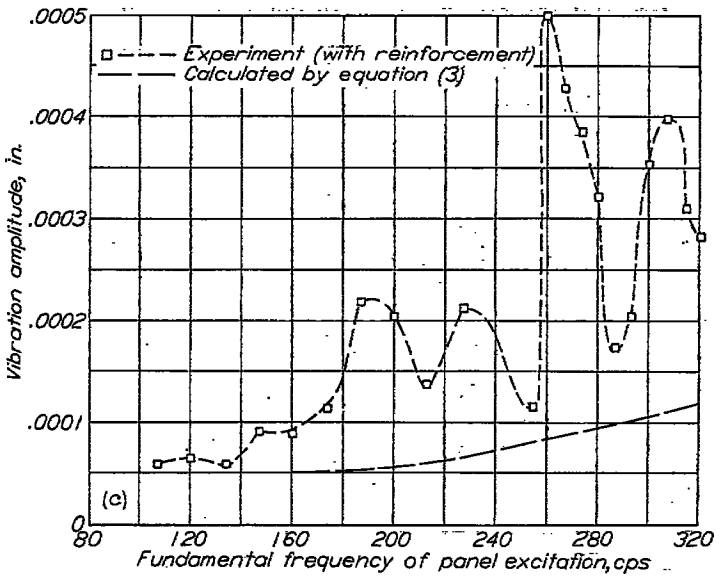

(c) Flat vertical wooden wall with four-blade propeller.

FIGURE 22.—Concluded.

Since the calculations were made for an assumed natural frequency of zero, the calculated curve does not indicate the response at resonance. A simple calculation such as this may be useful for predicting vibration amplitudes for heavy walls far from resonance.

For conventional fuselage walls, which weigh much less than those tested, the acoustical radiation resistance and damping cannot be neglected. A more refined method for calculating the response of an idealized panel and which gives the effect of rigidity, panel damping, and acoustical radiation resistance is given by equation 7 (b) of the appendix. This equation gives the vibration amplitude if the structural damping, mass, and natural frequency of the panel are known. Calculations for a resonant condition by equation 7 (b) have been made for comparison with experimental results and these values are shown in figure 22 (a). For these calculations, $f_0=130$ cycles per second, $\frac{C}{C_c}=0.02$ (estimated from shape of resonance peak), and the weight of the panel was 7 pounds per square foot. Equation 7 (b) shows that for lower values of the mass and frequency the acoustical radiation resistance becomes of greater importance. A conventional fuselage will therefore have greater damping and the resonances will not be so sharply peaked as in figures 22 (a) and 22 (b).

Effect of fuselage parameters on fuselage vibration.—The appendix shows that the panel vibration amplitude of the fuselage is a function of oscillating pressure and frequency as well as of mass, rigidity, and damping of the structure. Rigidity is effective in reducing low-frequency vibrations,

mass is the most effective in reducing high-frequency vibrations, and wall damping is the most effective in reducing the amplitude of the resonant peaks.

The present tests showed that the panel vibrated predominantly at the fundamental or lowest excitation frequency of the propeller. This fact has also been found to be the case for an airplane fuselage. Since rigidity is the most effective at the low frequencies, wall vibration may be reduced by increasing wall rigidity, provided, of course, that the resonant condition is far enough removed from the range in which the propeller operates. This increase in wall rigidity was accomplished for the test panels by means of reinforcements which raised the panel resonance frequency to a value higher than the fundamental excitation frequency. This procedure necessarily increases the possibility that the panel may be in resonance with the higher harmonics of the propeller. An inspection of figure 22 (c) shows that when the reinforced wooden panel was excited by the four-blade propeller several small resonances occurred at higher frequencies; however, these small resonances seemed to be of little importance.

Since the propeller has numerous exciting harmonics and the walls have numerous modes of vibration, eliminating all resonant conditions is impractical. It is therefore desirable to apply a damping material to the walls to reduce the amplitude of the resonant peaks.

The first section of the present report shows that as the tip Mach number is increased, more of the pressure energy goes into the higher harmonics. As indicated in the appendix, the mass of the wall becomes most effective in reducing wall vibration at the higher frequencies. The wall must therefore have sufficient mass to prevent excessive vibration at the high frequencies which predominate at high tip speeds.

SOUND LEVELS IN FUSELAGE

The difference in pressure level of sound as it passes into an enclosure such as a fuselage is given by reference 3 as

$$\text{Attenuation in decibels} = 10 \log_{10}\left(1 + \frac{A_c}{T_c}\right)$$

where A_c is the absorption coefficient in the enclosure and T_c is the transmission coefficient of sound through the walls. The transmission is given by the square of the ratio of wall vibration amplitude to the amplitude of the external sound wave. (See appendix.) The lower the wall vibration for a given external excitation, the lower is the transmission, and, hence, the greater the sound reduction. Such reduction is possible only if A_c is greater than zero; that is, only if sound-absorbing material is present in the fuselage can the sound intensity inside be less than the intensity outside. It may also be noted from the equation for attenuation that even though A_c be unity (its maximum value), the sound reduction will not be appreciable unless T_c is quite small. In the interest of crew comfort, a nominal value of absorption and a low value of transmission are therefore necessary.

The designer may reduce sound pressures in the fuselage: (1) by moving the engines outboard to increase tip clearance, (2) by increasing the number of blades, (3) by choosing the optimum fuselage shape, (4) by increasing fuselage rigidity, mass, and damping, and (5) by applying sound-absorbing material. Each of these variables is most effective over a certain range of conditions.

CONCLUSIONS

Free-space oscillating-pressure measurements for static conditions near the propeller tips (tip Mach number range 0.45 to 1.00) for five different propellers indicate the following conclusions:

1. Pressures measured on a line parallel to the propeller axis are increased as tip clearance is decreased; however, only the pressures in a region one-half radius ahead of the plane of rotation to one-half radius behind it are greatly increased.

2. At a constant power the pressure amplitudes of the lower harmonics tend to decrease and the higher harmonics tend to increase with an increase in tip Mach number. The fundamental frequency of pressure produced by a four-blade propeller is essentially independent of tip Mach number in the useful tip Mach number range.

3. Blade plan form and solidity do not seem to be significant parameters. Tip clearance divided by propeller diameter is shown to be significant.

4. At all tip Mach numbers the four-blade propeller produced smaller pressures than the two-blade propeller for the same power coefficient. At low tip Mach numbers these differences are large, whereas at tip Mach number 1.00, where a large amount of energy appears in the higher harmonics, they are relatively small.

5. A flat vertical wall in the pressure field approximately doubles the free-space pressures in the plane of the wall; a circular wall also increases the pressures but by a lesser amount.

6. Pressures of the fundamental frequency which impinge on the fuselage wall in front of the propeller plane tend to be out of phase with those behind the propeller plane.

7. At a constant power coefficient and at tip Mach numbers near 1.00, the pressure amplitudes are not appreciably reduced by increasing the number of blades; however, the resulting higher frequencies of the impinging pressures are beneficial in greatly reducing the vibration amplitude of the wall.

8. Oscillating pressures and their phase relations at any point in space may be predicted satisfactorily by the theory in this report. This analysis is primarily for use in the region near the propeller where the Gutin simplified solution is not valid.

LANGLEY AERONAUTICAL LABORATORY,
NATIONAL ADVISORY COMMITTEE FOR AERONAUTICS,
LANGLEY FIELD, VA., *February 18, 1949.*

APPENDIX

RESPONSE OF AN IDEALIZED PANEL TO A PLANE SOUND WAVE

The response of an idealized panel to a plane sound wave is given in reference 5, page 220. The panel is assumed to move as an infinite, thin, but rigid piston that can vibrate as a whole under the action of elastic and damping restraints. The equations are reproduced here in somewhat modified form to show the effect of rigidity, mass, and damping on the response of a panel.

The vibration velocity of the panel is given by the following equation:

$$\dot{\xi}_{02}e^{i\omega_1 t}=\frac{2K\dot{\xi}_{01}e^{i\omega_1 t}}{W} \qquad (4)$$

Substituting $K\dot{\xi}_{01}=p$ and $\dot{\xi}_{02}=i\omega_1\xi_{02}$ gives

$$\xi_{02}e^{i\omega_1 t}=\frac{2pe^{i\omega_1 t}}{i\omega_1 W} \qquad (5)$$

where

$$W=(C+2K)+i\left(M\omega_1-\frac{s}{\omega_1}\right)$$

The absolute value is given by

$$\xi_{02}=\frac{2p}{\omega_1\sqrt{(C+2K)^2+\left(M\omega_1-\frac{s}{\omega_1}\right)^2}} \qquad (6)$$

Utilizing the value of the critical damping for single-degree systems gives (p. 50, reference 6)

$$C_c=2M\omega_n$$

$$\xi_{02}=\frac{2p}{\omega_1\sqrt{\left(2\frac{C}{C_c}M\omega_n+2K\right)^2+\left(M\omega_1-\frac{s}{\omega_1}\right)^2}} \qquad (7a)$$

When $s=M\omega_n^2$ is substituted, equation (7a) may be written as

$$\xi_{02}=\frac{2p}{\omega_1\sqrt{\left(2\frac{C}{C_c}M\omega_n+2K\right)^2+M^2\omega_1^2\left[1-\left(\frac{\omega_n}{\omega_1}\right)^2\right]^2}} \qquad (7b)$$

For the case of zero damping, radiation resistance, and stiffness, equation (7a) reduces to

$$\xi_{02}=\frac{2p}{M\omega_1^2} \qquad (8)$$

This is the same equation as equation (3) in text with the exception of the factor 2. The pressure used in equation (3) is the pressure at the panel surface which for a large plane panel is double the free-space pressure because of reflection. The equations in this appendix are based on the free-space pressure of the incident wave.

The resonant condition of the panel is given by $\omega_1=\omega_n$. For this condition the amplitude of vibration is given by

$$\xi_{02}=\frac{p}{\frac{C}{C_c}M\omega_n^2+K\omega_n} \qquad (9)$$

The relation of the panel vibration amplitude to air amplitude at resonance may be written as

$$\frac{\xi_{02}}{\xi_{01}}=\frac{1}{1+\frac{C}{C_c}\frac{M\omega_n}{K}} \qquad (10)$$

Equation (10) shows that, if the structural damping $\frac{C}{C_c}$ is zero, the panel amplitude at resonance is equal to the amplitude of the impinging sound wave. The term $\frac{C}{C_c}\frac{M\omega_n}{K}$ must be greater than unity for the damping to make an appreciable difference in the amplitude. The value of this quantity for a typical fuselage having $\frac{C}{C_c}=0.10$, $M=0.8$ grams per centimeter^2, $\omega_n=2\pi 60=376$ radians per second, and $K=\rho c=42$ grams per centimeter^2-second is

$$\frac{C}{C_c}\frac{M\omega_n}{K}=\frac{(0.10)(0.80)(376)}{42}=0.70$$

Equation (10) shows that the damping is effective in reducing resonant peaks for high values of ω_n (high rigidity), mass, and damping coefficients. This equation indicates that damping reduces the amplitude of the higher responses but is not very effective in reducing the low-frequency peaks.

The transmission coefficient T_c of sound energy through a wall is given by the square of the ratio of wall amplitude to the amplitude of the impinging wave. The reciprocal of the transmission is given for the case of zero structural damping in reference 5 as

$$\frac{1}{T_c}=\frac{\left(M\omega_1-\frac{s}{\omega_1}\right)^2}{4\rho^2c^2}+1$$

where M is the mass of the wall per unit area, s is the stiffness ($s=M\omega_n^2$ where ω_n is natural frequency of panel), ω_1 is angular frequency of impinging sound, and c is velocity of sound in air.

This equation may be written for air at standard conditions (15° C and 760 mm. of Hg) as

$$T_c=\frac{7056}{7056+4\pi^2 f_1^2 M^2\left(1-\frac{f_0^2}{f_1^2}\right)^2} \tag{11}$$

where f_1 is the frequency of the impinging sounds, f_0, the natural frequency of the fuselage, and M, the mass per unit area of the fuselage.

REFERENCES

1. Gutin, L.: Über das Schallfeld einer rotierenden Luftschraube. Phys. Zeitscher. der Sowjetunion, Bd. 9, Heft 1, 1936, pp. 57–71.
2. Deming, Arthur F.: Propeller Rotation Noise Due to Torque and Thrust. NACA TN 747, 1940.
3. London, Albert: Principles, Practice, and Progress of Noise Reduction in Airplanes. NACA TN 748, 1940.
4. Nichols, R. H., Jr., Sleeper, H. P., Jr., Wallace, R. L., Jr., and Ericson, H. L.: Acoustical Materials and Acoustical Treatments for Aircraft. Jour. Acous. Soc. Am., vol. 19, no. 3, May 1947.
5. Davis, A. H.: Modern Acoustics. G. Bell and Sons Ltd. (London), 1934.
6. Den Hartog, J. P.: Mechanical Vibrations. Second ed., McGraw-Hill Book Co., Inc., 1940.

CONTENTS